

Surrogate Modeling and Explainable Artificial Intelligence for Complex Systems: A Workflow for Automated Simulation Exploration

Paul Saves^{1*}, Pramudita Satria Palar², Muhammad Daffa Robani³, Nicolas Verstaevel¹, Moncef Garouani¹, Julien Aligon¹, Benoit Gaudou¹, Koji Shimoyama⁴, Joseph Morlier⁵

¹*IRIT, UMR 5505 CNRS, Université Toulouse Capitole, Toulouse, 31000, France.

²Faculty of Mechanical and Aerospace Engineering, Institut Teknologi Bandung, Jl. Ganesha 10, Bandung, 15414, West Java, Indonesia.

³AwanTunai, Urban Suites, 3 Hullet Road, Singapore, 229158, Singapore, Singapore.

⁴Mechanical Engineering, Kyushu University, 744 Motooka, Fukuoka, 819-0395, Japan.

⁵Institut Clément Ader (ICA), Université de Toulouse, ISAE-SUPAERO, Mines Albi, UPS, INSA, CNRS, 3 rue Caroline Aigle, Toulouse, 31400, Occitanie, France.

*Corresponding author(s). E-mail(s): paul.saves@irit.fr;

Contributing authors: pramsp@itb.ac.id; daffa@awantunai.com; nicolas.verstaevel@irit.fr; moncef.garouani@irit.fr; julien.aligon@irit.fr; benoit.gaudou@ut-capitole.fr; shimoyama@mech.kyushu-u.ac.jp; joseph.morlier@isae-supero.fr;

Abstract

Complex systems are increasingly explored through simulation-driven engineering workflows that combine physics-based and empirical models with optimization and analytics. Despite their power, these workflows face two central obstacles: (1) high computational cost, since accurate exploration requires many expensive simulator runs; and (2) limited transparency and reliability when decisions rely on opaque blackbox components.

We propose a workflow that addresses both challenges by training lightweight emulators on compact designs of experiments that (i) provide fast, low-latency approximations of expensive simulators, (ii) enable rigorous uncertainty quantification, and (iii) are adapted for global and local Explainable Artificial Intelligence (XAI) analyses.

This workflow unifies every simulation-based complex-system analysis tool, ranging from engineering design to agent-based models for socio-environmental understanding. In this paper, we propose a comparative methodology and practical recommendations for using surrogate-based explainability tools within the proposed workflow. The methodology supports continuous and categorical inputs, combines global-effect and uncertainty analyses with local attribution, and evaluates the consistency of explanations across surrogate models, thereby diagnosing surrogate adequacy and guiding further data collection or model refinement. Additional contributions include an algorithmic workflow for coupling designs of experiments, emulator training, uncertainty propagation, and explanation generation, together with guidelines for selecting surrogate families under computational and interpretability constraints.

We demonstrate the approach on two contrasting case studies: a multidisciplinary design analysis of a hybrid-electric aircraft and an agent-based model of urban segregation. Results show that the surrogate–XAI coupling enables large-scale exploration in seconds, uncovers nonlinear interactions and emergent behaviors, identifies key design and policy levers, and signals regions where surrogates require more data or alternative architectures. These elements advance scalable, trustworthy, and explainability-driven automated machine learning for complex-system simulation and design exploration.

Keywords: Surrogate models · Explainable Artificial Intelligence · Complex systems simulations · Machine learning · Blackbox analysis · Agent-based modeling · Multidisciplinary design analysis.

1 Introduction

Modern engineering challenges in complex system modeling, ranging from electric aircraft design to urban infrastructure planning, are increasingly being tackled using simulation-driven approaches [39, 72].

A complex system is defined as one composed of many interconnected and interdependent elements whose nonlinear interactions give rise to emergent behaviors that cannot be directly inferred from the properties of the individual parts [56]. Such systems typically display emergent behaviors, self-organization, adaptation, and feedback loops, which make them challenging to capture holistically.

In the context of Agent-Based Modeling (ABM), simulations are often used to model ill-defined and context-sensitive dynamics where controlled experimentation is infeasible [1]. Although Simulations of Agent-Based Model (SABM) reproduce bottom-up emergence effectively, their flexibility and opacity raise credibility and interpretability challenges, presenting barriers for decision support and policy alignment [13]. The challenges of credibility and interpretability in SABM are not unique to agent-based approaches; many stochastic blackbox simulators face similar issues [6]. To manage these, formal modeling, verification, and trade-space analysis are employed, not only to evaluate designs but also to shape possibilities in response to evolving objectives and constraints [19].

For both modeling and understanding, we adopt an iterative “co-design” approach. While co-design can apply to other processes and contexts [105], here it denotes a twofold workflow. First, it aligns the diverse stakeholders and experts involved in complex system design that negotiate trade-offs across disciplines and establish a shared modeling ground [19] and, second, it coordinates participants around shared experimental materials such as models, scenarios, and data, so that agent roles, assumptions, and artefacts are jointly developed, interrogated, and analyzed to support an informed decision-making process [32]. These co-design processes require continuous trade-off balancing fidelity, computational cost, interpretability, and operational realism. Because these stochastic simulators often behave as opaque and blackboxes due to their inherent complexity and nonlinear dynamics, they can be difficult to understand, even when composed of simple and transparent rules. Consequently, there is a growing interest in embedding explainability, interpretability, and user-centric design [100]. As they expand in size and complexity, the demand for dedicated automated tools increases alike. Moreover, since these simulations are typically computationally expensive and can only be queried a limited number of times, careful selection of inputs through design of experiments or active learning is essential to maximize their utility under tight computational budgets. Simulation toolkits go beyond purely analytical purposes, serving as interactive, participatory platforms where diverse stakeholders, including engineers, decision makers, and domain experts, collaborate on the sustainable design or analysis of complex systems [20, 32].

This article explores the motivations, methods, and applications of surrogate modeling for simulations, emphasizing the trade-offs between accuracy, computational efficiency, and interpretability. This paper is also motivated by the pressing need to bridge predictive power and interpretability. We propose a workflow in which Explainable AI (XAI) is embedded into a surrogate-based simulation workflow to enable simple and fast workflows [42]. Surrogate models such as Gaussian processes, decision-tree ensembles, or lightweight neural networks approximate expensive simulation outputs using just a handful of high-fidelity runs (typically a few dozen). XAI techniques like SHAP, LIME, partial dependence plots, and sensitivity analysis are then applied to these surrogates to gather knowledge over the blackbox model, revealing how each input parameter may influence outcomes at both global and individual levels [73, 43], therefore enabling both frugal and explainable AI.

This workflow is generic and can be applied to many applications, therefore unifying the automated exploration of simulations, whether they represent an engineering design task or a complex system behavior analysis. We illustrate our framework with two contrasting case studies. The first one, from engineering and design, is based on a deterministic simulator whose equilibrium existence is guaranteed for admissible designs; the objective is the optimization of a given quantity of interest from the model. The second one consists of a stochastic multi-agent model and is based on a stochastic simulator whose equilibria depend on input values; the objective is the sensitivity analysis and mechanistic explanation of the system. Despite their different mathematical character, both problems are analyzed with the same methodology, demonstrating the applicability across domains of this work.

This work contributes to the growing field of explainable surrogate modeling for complex system simulations by bridging advances in machine learning, uncertainty quantification, and design exploration. Our contributions are structured along four main axes:

- (1) **Unified and explainable simulation workflow.** We introduce a methodological framework that integrates Explainable Artificial Intelligence (XAI) techniques directly into surrogate-assisted simulation workflows. The simulation-centric framework unifies simulators with diverse objectives

into a single iterative co-design loop, enabling transparent, interpretable, and efficient analysis of stochastic, high-dimensional models through automated XAI.

- (2) **Local and global XAI complementarity.** We clarify how global and local explanations play complementary roles in surrogate-assisted simulation: global analyses (feature effects, sensitivity, uncertainty) reveal system-level relationships, while local attributions (instance-level importance scores) explain individual predictions and highlight actionable drivers. We introduce simple metrics to compare explanations across surrogate models and the original simulator, detect divergences, and guide active sampling and model refinement.
- (3) **Comparison and recommendation of surrogate-based explainability tools.** Building on surrogate models and XAI techniques that handle both continuous and categorical features, we propose a formal comparative methodology to assess surrogate adequacy. The methodology comprises global and local effect analyses and evaluates how consistently different surrogate models generate explanations.
- (4) **Evaluation and insights across domains.** We demonstrate the approach on two representative case studies: (*i*) a multidisciplinary engineering design optimization problem, where surrogate models reveal system-level trade-offs and sensitivities, and (*ii*) an agent-based analysis and exploration scenario, where surrogate-based XAI uncovers behavioral drivers and emergent macro-patterns. From these studies, we identify complementarities and discrepancies between local and global explanations and across surrogate models, and we provide guidelines and perspectives for future research and applications.

The remainder of this paper is organized as follows. Section 2 reviews the state of the art on explainable AI for simulations, covering surrogate modeling approaches, explainability techniques, and the concepts underpinning their integration. Section 3 presents the proposed unified methodology that combines simulation-based modeling, surrogate learning, and interpretability analysis within an iterative co-design workflow. Section 4 applies this framework to a multidisciplinary aircraft design study, illustrating how interpretable surrogate models can accelerate exploration and uncover engineering insights in the DRAGON hybrid-electric aircraft. Section 5 applied the workflow to a socio-technical domain through an agent-based urban segregation model, highlighting how surrogate-assisted explainability supports policy assessment and uncertainty analysis. Finally, Section 6 concludes the paper and outlines future perspectives for embedding interpretability and co-design principles into next-generation simulation workflows.

2 Related work on explainable AI for simulations

Engineering simulators, such as computational fluid dynamics or multidisciplinary design analysis, approximate coupled governing equations to predict a complex physical behavior, enabling detailed performance and reliability assessment in highly nonlinear settings [94, 74, 9, 30]. Complementarily, SABM adopt a bottom-up perspective: heterogeneous agents following local decision rules interact over spatial or networked environments to produce emergent, multi-scale dynamics applied to epidemic forecasting, urban planning, infrastructure management, flood mitigation, and more [68, 57, 25]. Overall, modern simulators, whether physics-based or agent-based, face common challenges: high evaluation cost, mixed continuous and categorical inputs, strong nonlinearity, and limited transparency of causal mechanisms [32, 83]. These challenges have driven rapid progress in coupling surrogate modeling with explainable AI (XAI) methods that can scale explanation and uncertainty quantification to expensive simulators [41, 5].

In this section, we survey the literature on surrogate-based XAI for complex system simulations, with particular emphasis on methodological advances in surrogate modeling and local or global explainability techniques.

2.1 Surrogate models

Surrogate models, also known as metamodels or emulators, provide fast approximations of expensive blackbox simulations. They are trained on a carefully designed set of high-fidelity runs, often generated with a DoE strategy such as Latin Hypercube or Sobol' sampling, and evaluated through the expensive opaque simulator whose mechanisms we seek to uncover [66, 11]. Building an emulator involves optimizing its parameters to best reproduce the simulator outputs, for example, by maximizing the likelihood of the observed data [78]. Once trained, the surrogate model can be evaluated quickly, making it suitable to

replace the expensive simulator in optimization loops, sensitivity analyses, or uncertainty quantification studies [28, 33]. Common surrogate models include Gaussian process regression (Kriging), radial basis function networks, multivariate adaptive regression splines, neural networks, and tree ensembles; each offers different trade-offs in accuracy, interpretability, and computational cost [1]. In principle, almost any machine learning model can serve as an emulator. However, surrogate models are typically designed with specific goals in mind, such as uncertainty quantification or interpretability. Also, the surrogate models should account for limited training data and be tailored to approximate expensive simulators efficiently. Advanced strategies, such as multi-fidelity modeling, gradient-enhanced Kriging, and adaptive sampling via active learning, further improve surrogate precision while minimizing the number of expensive simulator calls [81]. Some models come with intrinsic uncertainty quantification like Gaussian processes (posterior variance), random forest ensembles (prediction intervals), or transformer-based predictors (*e.g.* TabPFN). Some models come with derivative-based methods (*e.g.* polynomial chaos expansions or kernel-based surrogate models) that support coupled systems emulation through adjoint-based methods [88, 70]. In the context of agent-based modeling, previous works [38] used machine learning surrogates to accelerate ABM parameter sweeps while maintaining interpretable mappings between inputs and outputs, enabling practical calibration workflows [1]. By substantially reducing simulation costs, often by several orders of magnitude, surrogate modeling enables comprehensive exploration of high-dimensional design spaces, facilitates global sensitivity analyses, and supports robust, real-time decision-making. Across engineering and agent-based modeling domains, these emulators transform previously intractable scenarios into computationally efficient and reliable workflows.

Notations

Let the feature indices be $\{1, \dots, n\}$ and let an input point \mathbf{x} be such that $\mathbf{x} = [x_1, x_2, \dots, x_n]^\top \in \Omega = \prod_{i=1}^n \Omega_i$ where each feature i may be either continuous, integer ($x_i \in \{a_1, \dots, a_k\}$), or categorical ($x_i \in \{c_1, \dots, c_l\}$) [86]. An integer variable is ordered (*e.g.* $a_4 < a_5 < a_6$) while the values that a categorical variable can take, termed “levels”, are generally considered without intrinsic order. The quantity of interest y is related to an input \mathbf{x} via a blackbox simulator $y = f(\mathbf{x})$, which we approximate by $\hat{f}(\mathbf{x}) \approx y$ using the dataset of m points denoted $\mathcal{D} = \{\mathcal{X}, \mathcal{Y}\}$. Here, $\mathcal{X} = \{x_j^{(i)}\}_{j=1 \dots n}^{i=1 \dots m}$ is a chosen Design of Experiment (DoE) (*e.g.* a small Latin hypercube or Sobol’ sampling), $\mathcal{Y} = \{f(\mathbf{x}^{(i)})\}_{i=1}^m$ are the corresponding simulator outputs [11] and $\hat{f} : \Omega \rightarrow \mathbb{R}$ is the fast-to-evaluate emulator of f . Building an emulator consists in training $\hat{f}(\mathbf{x} | \mathcal{D}, \Theta)$ by learning optimal surrogate model hyperparameters Θ , for example by maximizing the likelihood of the data \mathcal{D} given hyperparameter Θ [78]. Once trained, $\hat{f}(\mathbf{x})$ is a fast-to-evaluate surrogate that can replace costly simulations within optimization loops or uncertainty quantification studies [28, 33].

Model validation

To provide a unified assessment of surrogate model quality, we combine complementary metrics that are conceptually and practically linked: pointwise accuracy for numerical fidelity, classification reliability for feasibility or constraint predictions, uncertainty calibration for safe decision making, and ranking consistency for interpretability.

The pointwise error is measured by the Root Mean Square Error (RMSE) on another dataset called the validation set \mathcal{D}_{val} consisting of m_{val} blackbox evaluations,

$$\text{RMSE} = \sqrt{\frac{1}{m_{\text{val}}} \sum_{i=1}^{m_{\text{val}}} (y_i - \hat{f}(x^{(i)}))^2}, \quad (1)$$

which quantifies the average magnitude of residuals and thereby serves as the baseline indicator of numerical precision [4].

For problems that involve binary outcomes (*e.g.* feasible/infeasible, constraint satisfied / violated), we complement RMSE with a balanced classification metric, the Matthews Correlation Coefficient (MCC),

$$\text{MCC} = \frac{TP \cdot TN - FP \cdot FN}{\sqrt{(TP + FP)(TP + FN)(TN + FP)(TN + FN)}}, \quad (2)$$

Because MCC synthesises the confusion matrix into a single correlation-like score that remains meaningful under class imbalance [23] (note that MCC is undefined when any denominator term is zero).

Beyond point estimates and categorical accuracy, reliable uncertainty estimates are essential for Bayesian assessment or risk-aware design; we therefore evaluate variance calibration with the Predictive Variance Adequacy (PVA),

$$\text{PVA} = \left| \log \left(\frac{1}{m_{\text{val}}} \sum_{i=1}^{m_{\text{val}}} \frac{(y_i - \hat{f}(x^{(i)}))^2}{\hat{\sigma}_i^2} \right) \right|, \quad (3)$$

where $\hat{\sigma}_i^2$ is the model's predictive variance for sample i ; values near zero indicate well-calibrated uncertainty, while large deviations reflect either overconfidence or underconfidence and motivate recalibration or richer probabilistic models [10].

2.2 Explainable AI

Explainable Artificial Intelligence (XAI) comprises methods and practices aimed at rendering machine-learning and simulation models transparent and their outputs intelligible to human users; its central aim is to clarify how inputs, model structure, and uncertainty lead to particular predictions or decisions. Important distinctions in XAI include intrinsic versus post-hoc approaches: intrinsic models are interpretable by design, whereas post-hoc methods generate explanations after training to illuminate blackbox behavior. Another key distinction is global versus local explanations: global methods characterize system-level behavior and dominant input–output relationships, while local methods provide instance-specific rationales useful for debugging, risk assessment, and actionable decision support [69]. A representative technique for global explainability is Global Sensitivity Analysis (GSA), for example, Sobol' indices, which quantify how input uncertainties contribute to output variability, thereby guiding feature prioritization and robustness assessment [97, 84]. For local explainability, XAI generally conveys influence details with instance-based methods such as with SHAP (SHapley Additive exPlanations), LIME (Local Interpretable Model-agnostic Explanations), or counterfactual explanations [59, 98]. These model-agnostic tools assign credit to input features at the local prediction level [73], producing human-readable explanations or actionable change suggestions.

Explainable Artificial Intelligence (XAI), when integrated with surrogate modeling, provides an effective framework to address the interpretability challenges of complex systems. Surrogate models enable the efficient evaluations and systematic exploration required for explainability analyses [1, 9]. Yet, without suitable interpretability tools, surrogates may themselves act as blackboxes. The key objective remains to explain the behavior of the underlying complex system rather than the surrogate model itself, especially since many XAI methods focus on the surrogate without distinguishing between explanations based on raw data and those arising from the surrogate's internal structure and therefore introducing another level of bias and uncertainty [44, 17]. On the visual aspects, surrogate models allow for computing Partial Dependence Plots (PDP) and Individual Conditional Expectation (ICE) quickly to reveal marginal and instance-level effects of variables on model predictions, even in the presence of complex interactions [46, 40]. For instance, in [45], the authors propose a surrogate model framework that autonomously approximates a robotic agent's behavior and uses feature-attribution together with a natural-language generation pipeline to produce human-readable explanations, validated on simulated and real industrial data.

Notations

Let the feature indices $N = \{1, \dots, n\}$ be partitioned into two disjoint subsets: A (variables of interest) and C (complement). Also, let $\mathbf{x} = (\mathbf{x}_A, \mathbf{x}_C)$ with $\mathbf{x}_A \in \Omega_A$ and $\mathbf{x}_C \in \Omega_C$ and P_{X_C} denote the marginal law of X_C . The partial dependence function of \hat{f} on \mathbf{x}_A is

$$\hat{f}_A(\mathbf{x}_A) = \mathbb{E}_{X_C \sim P_{X_C}} [\hat{f}(\mathbf{x}_A, X_C)] = \int_{\Omega_C} \hat{f}(\mathbf{x}_A, x_C) dP_{X_C}(x_C).$$

Evaluating \hat{f}_A over Ω_A yields the *Partial Dependence Plot* (PDP), which visualizes the average effect of \mathbf{x}_A on \hat{f} . A simple global sensitivity metric for the i -th feature is the variance of its one-dimensional PDP:

$$\sigma_{\text{pd},i}^2 = \mathbb{V}[\hat{f}_i(x_i)].$$

For continuous or ordinal variables, this variance quantifies the magnitude of influence of x_i on the model output. However, for categorical variables, the notion of variance is not directly meaningful because categories lack a natural ordering. In such cases, a practical heuristic alternative sensitivity measure is the (normalized) range of the partial dependence values:

$$\sigma_{\text{pd},i} = \frac{\max_{x_i \in \mathcal{X}} \hat{f}_i(x_i) - \min_{x_i \in \mathcal{X}} \hat{f}_i(x_i)}{4}. \quad (4)$$

When interactions or non-stationarities are present, PDPs may obscure important local variations. *Individual Conditional Expectation* (ICE) plots address this issue by conditioning on each observed background instance $\mathbf{x}_C^{(j)}$ and displaying

$$\hat{f}_A^{(j)}(\mathbf{x}_A) = \hat{f}(\mathbf{x}_A, \mathbf{x}_C^{(j)}), \quad j = 1, \dots, m.$$

The collection $\{\hat{f}_A^{(j)}\}_{j=1}^m$ reveals the spread of individual responses around the PDP mean. Note that PDP and ICE rely on (marginal) input independence; strong input correlations can render these visualizations misleading, and call for conditional partial dependence, ALE plots, or other dependence-aware alternatives [2]. Still, most surrogate models employ space-filling DoEs and are based on the input-independence assumption [76], making PDP/ICE visualizations and sensitivity tools fitted for this context [61]. Notwithstanding, a better practice is to test input independence beforehand on the dataset [7].

The Shapley value, originally introduced in cooperative game theory [92], provides an axiomatic rule to fairly attribute a total payoff to individual players. Let N denote the set of players (features) and $v : 2^N \rightarrow \mathbb{R}$ a value function that assigns a payoff to each coalition $S \subseteq N$. The Shapley value of player $i \in N$ is

$$\Phi_i(v) = \sum_{S \subseteq N \setminus \{i\}} \frac{|S|!(n - |S| - 1)!}{n!} (v(S \cup \{i\}) - v(S)), \quad (5)$$

which equals the average marginal contribution of i over all possible coalitions and satisfies the classical Shapley axioms (efficiency, symmetry, dummy, additivity).

The SHAP framework [67] adapts this principle to model explanations by treating features as players and the model prediction as the payoff. For a predictive model \hat{f} and a specific instance \mathbf{x} , define the instance-specific value function

$$v_{\mathbf{x}}(S) = \mathbb{E}[\hat{f}(\mathbf{X}) \mid \mathbf{X}_S = \mathbf{x}_S], \quad S \subseteq N,$$

where the expectation is taken with respect to a chosen background distribution for \mathbf{X} (the choice of which must be reported in practice). The SHAP value (feature attribution) of the feature i , for instance \mathbf{x} is obtained by applying (5) to $v_{\mathbf{x}}$:

$$\phi_i(\mathbf{x}) = \sum_{S \subseteq N \setminus \{i\}} \frac{|S|!(n - |S| - 1)!}{n!} (v_{\mathbf{x}}(S \cup \{i\}) - v_{\mathbf{x}}(S)). \quad (6)$$

By construction, the SHAP values provide the additive decomposition

$$\hat{f}(\mathbf{x}) = v_{\mathbf{x}}(\emptyset) + \sum_{i=1}^n \phi_i(\mathbf{x}),$$

where $v_{\mathbf{x}}(\emptyset)$ is the prediction of the baseline (reference). To capture pairwise interactions, SHAP introduces interaction values $\phi_{i,j}(\mathbf{x})$ for $i \neq j$. One convenient symmetric definition is

$$\phi_{i,j}(\mathbf{x}) = \frac{1}{2} \sum_{S \subseteq N \setminus \{i,j\}} \frac{|S|!(n - |S| - 2)!}{(n - 1)!} (v_{\mathbf{x}}(S \cup \{i,j\}) - v_{\mathbf{x}}(S \cup \{i\}) - v_{\mathbf{x}}(S \cup \{j\}) + v_{\mathbf{x}}(S)), \quad (7)$$

which yields $\phi_{i,j}(\mathbf{x}) = \phi_{j,i}(\mathbf{x})$ and decomposes each feature attribution as

$$\phi_i(\mathbf{x}) = \sum_{j=1}^n \phi_{i,j}(\mathbf{x}).$$

The main (non-interaction) effect of feature i is then commonly defined by

$$\phi_{i,i}(\mathbf{x}) = \phi_i(\mathbf{x}) - \sum_{j \neq i} \phi_{i,j}(\mathbf{x}),$$

so that the full decomposition across main effects and pairwise interactions is coherent and sums to the model prediction difference $\hat{f}(\mathbf{x}) - v_{\mathbf{x}}(\emptyset)$.

Practical computation of the expectations $v_{\mathbf{x}}(S)$ requires a choice of background distribution and typically relies on approximations (sampling, model-specific fast algorithms, or conditional expectation estimators) due to the combinatorial number of subsets. These implementation choices affect both the numerical values and the interpretation of SHAP attributions and should therefore be reported alongside any SHAP-based analysis [67, 52, 29].

A commonly used global importance score for feature i is the expected absolute SHAP value:

$$S_i = \mathbb{E}[|\phi_i|] \approx \frac{1}{m} \sum_{j=1}^m |\phi_i^{(j)}|,$$

which aggregates instance-level contributions into a summary ranking of feature importance across the dataset [73, 64].

Model validation

Because surrogate models are often used as interpretable metamodels of a more complex simulator, we check whether the surrogate preserves feature-importance structure using a ranking agreement metric based on SHAP values: the Normalized Discounted Cumulative Gain (NDCG). Let $\text{rel}_{i,j}$ be the absolute SHAP magnitude of sample i for the j -th ranked feature ; then, for two models \mathcal{M}_1 and \mathcal{M}_2 :

$$\text{DCG}_i = \sum_{j=1}^n \frac{\text{rel}_{i,j}}{\log_2(j+1)}, \quad \text{NDCG}_{\mathcal{M}_1, \mathcal{M}_2} = \frac{1}{m} \sum_{i=1}^m \frac{\text{DCG}(\mathcal{M}_1)_i}{\text{DCG}(\mathcal{M}_2)_i}, \quad (8)$$

where values close to 1 indicate that the surrogate preserves the reference model's explanation ranking [15].

2.3 Previous works

The workflow and applications presented in this paper build upon our previous studies, where we applied surrogate-based explainable AI (XAI) using SHAP-enhanced surrogate models to multi-objective aerodynamic design problems. These studies demonstrated that SHAP provides more detailed and nuanced insights than traditional sensitivity analysis techniques, such as Sobol' indices or active subspaces [74]. Furthermore, we developed, within the Surrogate Modeling Toolbox (SMT) framework [88, 83], a toolbox named SMT-EX (SMT for Explainability), which integrates SHAP, partial dependence plots (PDP), and individual conditional expectation (ICE). SMT-EX is effective for both continuous and mixed-categorical design spaces and enables systematic and straightforward extraction of design insights. In particular, SHAP is central to our approach, as Shapley values offer a rigorous method for fairly allocating the total variance of a coalition among the input features [92]. Note that, in earlier work [87], we investigated automated, data-based, active learning for the simulation problem of Section 4. Notably, in the Bayesian setting, a surrogate model trained on a given dataset can evaluate its own uncertainty and, through active learning (*e.g.*, Bayesian optimization), propose additional simulation points where its predictions are least certain. By iterating between surrogate fitting and targeted sampling, the model quickly learn in on the most critical regions of the response surfaces with a minimal number of runs [94]. When the chosen stopping criterion is met, generally a computational budget, one can use the final dataset to train several surrogate models to obtain insights to understand and analyze the blackbox model. This being out of the scope of this paper, in the following, active learning will not be further addressed hereinafter.

In summary, surrogate models speed up the extraction of data-driven insights, support quantitative analysis of complex systems under uncertainty, and make it feasible to evaluate computationally expensive metrics that characterize model behavior. Paired with XAI, surrogate models therefore enhance the interpretability and explanatory reach of simulation studies. Accordingly, our workflow replaces the true simulator f by its surrogate \hat{f} whenever we compute XAI measures or uncertainty estimates. While

the canonical definitions of the relevant quantities are given with respect to f , direct evaluation on f is typically intractable; instead, we compute their surrogate approximations via \hat{f} . This substitution introduces an unavoidable *epistemic uncertainty* that captures the unknown discrepancy between \hat{f} and f and which we account for in our analyses [71].

In summary, surrogate-based XAI operates at two complementary levels. At the local level, instance-wise analyses probe specific configurations to check reliability (e.g., exceedance probabilities), identify tipping points, and assess decision-relevant risk. These analyses typically require targeted resampling in regions of interest. At the global level, aggregated analyses quantify dominant drivers, nonlinear effects, and trade-offs across the input domain using variance- or dependency-based sensitivity indices [75]; global analyses generally rely on space-filling DoEs for broad coverage.

Both levels demand rigorous validation: predictive fidelity, calibration of uncertainty estimates, and stability of explanations should be verified, preferably across multiple surrogate families or via selective high-fidelity reevaluation. We use the four measures introduced earlier jointly: RMSE to compare regressors, MCC to flag classification weaknesses, PVA to validate uncertainty-driven acquisition, and NDCG to check that surrogate-derived explanations remain faithful to the high-fidelity model.

The primary objective of this work is to leverage these explainability metrics to make complex simulation models more interpretable, trustworthy, and actionable within co-design processes—while using surrogate models to reduce the computational cost of large-scale exploration. A detailed methodology for doing so is described in the following section.

3 Framework

Our methodology aims to unify simulation-based modeling, machine learning surrogate models, and interpretability analysis within a single unifying workflow. The approach addresses the challenge of exploring and designing complex system models with respect to an inherently unknown or partially observable ground truth. It builds upon the idea that simulation and inference are complementary iterative processes rather than distinct stages of inquiry [101, 102]. Figure 1 summarizes the five key stages of the proposed workflow, colored in orange:

1. **Conceptual and physical modeling:** formalize mechanistic assumptions, boundary conditions, and modeling goals to ensure coherence with the underlying phenomenon while maintaining tractability.
2. **Design of Experiments (DoE):** select an initial, structured sampling plan (e.g., Latin hypercube, Sobol' sequence, or expert-guided sampling) reflecting prior knowledge and regions of epistemic importance.
3. **High-fidelity simulation:** build and implement a simulator to capture the model evolution. Then, evaluate the simulator at the previously selected input points, recording both outputs and noise or measurement characteristics.
4. **Surrogate modeling:** train interpretable, fast-to-evaluate surrogate models (e.g., Gaussian Processes, ensemble trees, or sparse neural networks) that encode prior information and quantify posterior uncertainty.
5. **Explainability and sensitivity analysis:** apply global (e.g., Sobol', HSIC, PDP) and local (e.g., SHAP, LIME) techniques to identify main effects, interactions, and stability of explanations.

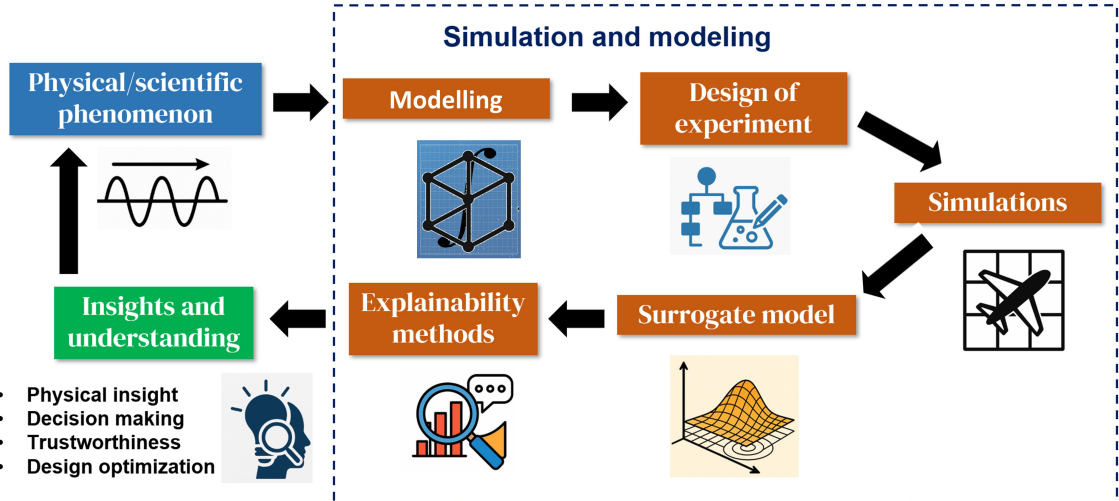


Fig. 1: Workflow for interpretable surrogate modeling in complex system co-design.

Priors should, whenever practicable, be elicited from domain knowledge (*e.g.*, physical bounds, expert judgement). Interpretable, computationally inexpensive surrogates are then introduced to transform costly, high-fidelity simulators into interactive co-design and decision-making tools across the system life cycle [37]. Our methodological stance is explicitly epistemic: models and simulations are treated as approximate, *a priori* constructs whose utility is assessed through probabilistic inferences and iterative simulation processes [101]. Explicit identification and quantification of prior assumptions, modeling errors, and approximation gaps are therefore central to the workflow. Moreover, modeling choices encode prior beliefs—about mechanisms, plausible parameter ranges, and relevant scales—and introduce structural approximations that require assessment.

We distinguish four sources of uncertainty and error that the methodology explicitly addresses [58]. First, hidden variables uncertainty, arising from intrinsic stochasticity within the system or simulator, for instance, the seed parameter in a pseudo-random socio-technical simulation. Second, data-related uncertainty, due to limited, noisy, or incomplete observations and unobserved factors. Third, model discrepancy, corresponding to the mismatch between the simulator’s structural assumptions and the target phenomenon, for example, an unwarranted independence assumption between variables. Finally, surrogate approximation error refers to the residual gap between surrogate predictions and high-fidelity simulator outputs. For instance, a model can perform poorly in terms of accuracy but remains useful and interpretable. Framing these uncertainties within a Bayesian perspective enables coherent expression of *a priori* knowledge and systematic belief updating as new simulation data are acquired [80]. Even deterministic simulations reflect choices of formalism, scale, and representation in their structures, leading to underlying decisions that affect how surrogate-based explanations are later constructed, presented, and understood [102]. Consequently, it is essential to verify that surrogate approximation error is acceptably small for the intended exploration task and that the chosen design of experiments provides sufficient coverage for the planned validation [104].

This framework supports two main research objectives: (i) How can surrogate models provide a local, instance-wise understanding of complex models? (ii) What global insights can they reveal about model dynamics and structural behavior? In summary, the proposed methodology transforms costly, high-fidelity simulations into transparent supports for reasoning, co-design, and decision-making across the system life cycle [17, 37]. In the next sections, we demonstrate through experiments how these tools enable systematic exploration of simulation behaviors and user-oriented analysis. Section 4 presents the application of our workflow to goal-oriented design of a complex system, and Section 5 presents the application of our framework to policy assessment and robust analysis of a complex system.

4 Engineering Insights from Multidisciplinary Design Exploration

Multidisciplinary Design Analysis and Optimization (MDAO) integrates models from different engineering domains to study trade-offs and interactions in complex systems across potentially conflicting engineering disciplines. Figure 2 integrates surrogate models into a co-design-oriented simulation process. This is an instance of the workflow introduced in Fig. 1, specifically instantiated for this engineering

problem. It begins with the definition of the Multidisciplinary Design Analysis (MDA) integrated model and the generation of a static Design of Experiments across the input space of the aircraft configuration, encompassing key geometric and operational parameters, including mixed categorical variables.

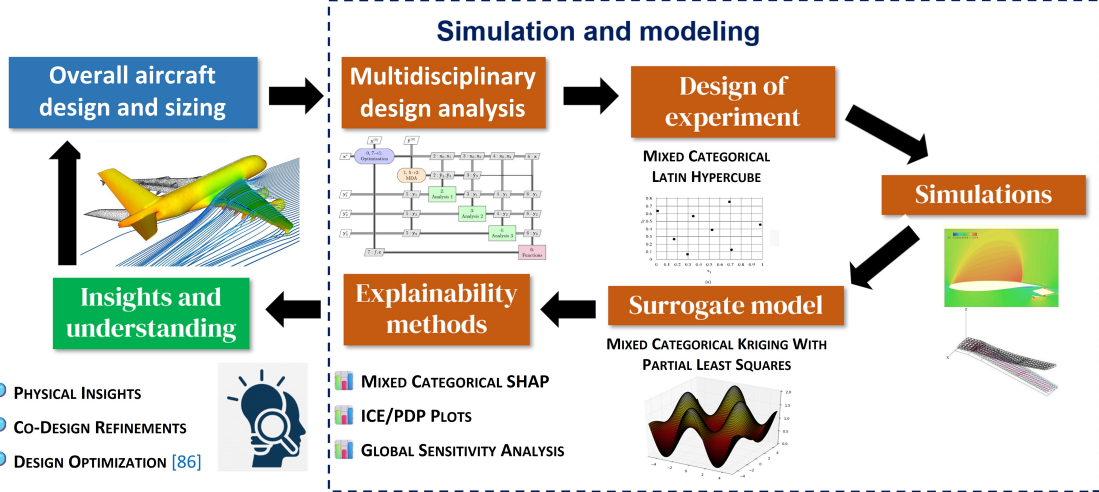


Fig. 2: Workflow for interpretable surrogate models for a design-oriented simulation.

Each configuration is evaluated using a high-fidelity simulator to obtain target outputs, including fuel mass. A surrogate model is then trained on this dataset to emulate the costly simulator with substantially reduced computational cost. XAI techniques are applied to the surrogate to quantify the influence of individual design variables on fuel mass. These insights inform stakeholders during the co-design process, guiding refinements and highlighting trade-offs between competing objectives and constraints, such as energy performance and passenger capacity. This section demonstrates how our simulation workflow can be applied to the sequential design of a complex system, integrating explainability, and extending our previous work [85] by handling mixed-variable input spaces, whereas most existing approaches are restricted to continuous variables.

First, Section 4.1 introduces the physical engineering design of interest and describes its main geometric and operational design variables together with the equilibrium target. After that, the workflow unfolds as described in Fig. 2. Section 4.2 then describes the modeling approach for coupling multidisciplinary submodels in a co-design frame; Section 4.3 introduces the Design of Experiments for the mixed continuous/categorical space and the aggregated output metrics used to train surrogates; Section 4.4 details the simulator implementation and numerical settings; Section 4.5 presents the surrogate model, and Section 4.6 reports the global and local XAI analyses, highlighting key interactions and trade-offs.

4.1 Overall aircraft design and sizing of a Hybrid-Electric aircraft

For the first demonstration, we applied various explainability methods to the “DRAGON” configuration (Distributed fans Research Aircraft with electric Generators by ONERA) to investigate how the aircraft’s input variables influence fuel mass from the stakeholder point of view. This aircraft concept study is funded by the European Commission, aiming to design the next generation of long-range aircraft that reduces climate impact as measured via radiative forcing [55]. The DRAGON concept represents a distributed hybrid electric propulsion architecture, which combines multiple electrically driven fans with conventional gas turbines [82] whose mock-up is given in Fig. 3. Assessing such configurations demands high-fidelity coupling of electrical engineering, aerodynamic performance, thermal-structural integrity, fluid-structure interaction, flight mechanics, or system-level failure modes [79] and is generally modeled with an extended design structure matrix [60].



Fig. 3: DRAGON aircraft mock-up [82].

This distributed electric propulsion concept, proposed by ONERA in 2019, was developed to support the European CleanSky2 initiative, which targets a 30% reduction in CO₂ emissions by 2025. The DRAGON aircraft was designed to carry 150 passengers over a range of 2750 nautical miles at a cruise speed of Mach 0.78. While the configuration has previously been studied in the context of optimization for minimizing fuel mass [87], there has been no in-depth investigation into the relationships between the design variables and fuel mass, an aspect that this study aims to address using explainability analysis [85].

Because DRAGON is part of multidisciplinary and international research, its design process already involves extensive co-design among aerodynamics, propulsion, and structural disciplines to integrate multiple expert assessments and technology assumptions. It is a so-called *coupled system* whose objective is to find a co-design trade-off corresponding to a functioning equilibrate aircraft that respects a certain static margin while being able to fulfill its mission at a minimal speed and over a minimal range [96].

This problem features 10 continuous and 2 categorical input variables, in which the quantity of interest is fuel mass. The 10 continuous variables correspond to the geometrical and flight parameters of the aircraft as shown in Tab. 1. The first and second categorical variables correspond to the electric architecture with 17 levels and turboshaft layout level with 2 levels, respectively. The architecture variable and the turboshaft layout are defined in Tables 2 and 3, respectively.

Function/Variable	Nature	Range
Fan operating pressure ratio	cont	[1.05, 1.3]
Wing aspect ratio	cont	[8, 12]
Angle for swept wing	cont	[15, 40] (°)
Wing taper ratio	cont	[0.2, 0.5]
Horizontal Tail (HT) aspect ratio	cont	[3, 6]
Angle for swept HT	cont	[20, 40] (°)
HT taper ratio	cont	[0.3, 0.5]
Takeoff Field Length (TOFL) for sizing	cont	[1800, 2500] (m)
Top of climb vertical speed for sizing	cont	[300, 800] (ft/min)
Start of climb slope angle	cont	[0.075, 0.15] (rad)
Architecture (levels)	cat	{1, 2, ..., 16, 17}
Turboshaft layout (levels)	cat	{1, 2}

Table 1: Design variables for fuel mass analysis.

4.2 Multidisciplinary design analysis

Designing complex engineered systems, such as an aircraft, requires the coordinated work of several tightly coupled disciplines (aerodynamics, structures, propulsion, controls, etc.). A decision made in one subsystem, for example, a change in wing geometry, often triggers responses in others (drag, loads, engine demand), producing nonlinear interactions across multiple feedback loops. To tame this complexity, *eXtended Design Structure Matrix* (XDSM) diagrams provide a compact, yet expressive, graphical language for showing modules, data exchanges, solver loops, and execution order; these diagrams make it easy to spot which components must be solved iteratively and which can be treated more loosely [60]. Put simply, an XDSM is a schematic of the problem structure that helps teams see where coupling and iteration are required. These schematic descriptions can be converted into executable *Multidisciplinary Design Analysis and Optimization* (MDAO) workflows in frameworks such as OpenMDAO. In that setting, each discipline is wrapped as a component, drivers coordinate solvers and optimizers, and

Table 2: Definition of the architecture variable and its 17 associated levels.

Architecture number	number of motors	number of cores and generators
1	8	2
2	12	2
3	16	2
4	20	2
5	24	2
6	28	2
7	32	2
8	36	2
9	40	2
10	8	4
11	16	4
12	24	4
13	32	4
14	40	4
15	12	6
16	24	6
17	36	6

Table 3: Definition of the turboshaft layout variable and its 2 associated levels.

Layout	position	y ratio	tail	VT aspect ratio	VT taper ratio
1	under wing	0.25	without T-tail	1.8	0.3
2	behind	0.34	with T-tail	1.2	0.85

system-level derivatives or surrogate models are propagated to support efficient gradient-based exploration of the design space [47]. In plain terms, XDSM gives you the blueprint, and MDAO provides the assembly line to run experiments and optimizations automatically. Used together, they improve traceability and reproducibility, guide the choice of solvers and surrogate strategies, and enable faster, more disciplined trade studies before committing significant resources to costly high-fidelity simulations.

For modeling the electric architecture, it proves more effective to use two integer variables rather than a single categorical one to capture the design options. However, this choice significantly enlarges the space of possible architectures beyond the original 17 configurations. There are, nevertheless, two limitations that restrict this expanded domain. The first limitation is about how components are wired together because building a certifiable electrical topology is not simple. For example, deciding how to connect eight motors to six generators needs careful engineering. The second limitation concerns the distributed propulsion system and its many propellers. For safety and stability reasons, not every possible electrical connection is acceptable, and some arrangements would create too many potential failure modes. To keep the optimization manageable and avoid overcomplicating the constraint structure, the model ultimately reverts to a single categorical variable that encodes only the feasible and certified architectures.

4.3 Design of experiments and aggregated output metrics

We generate a 1000-point Design of Experiments (DoE) using a Latin Hypercube Sampling (LHS) that we adapted for mixed-variable spaces [88]. While we have also developed adaptations of other sampling methods, such as Sobol' sequences for mixed hierarchical variables [16], we consistently employ LHS in this study. This choice is due to its low-discrepancy properties, which, although slightly less optimal for variance approximation and uncertainty quantification compared to Sobol' sequences, offer a practical balance between efficiency and simplicity [62].

Also, we will consider only the fuel mass response as the targeted output, which is the total mass of fuel consumed by the aircraft during the mission as predicted by the simulator.

4.4 Implementation of the simulator

In our workflow, the abstract XDSM diagrams are converted into executable multidisciplinary design analysis (MDA) simulations that constitute the computational backbone of the DRAGON co-design model. These simulations couple aerodynamic, structural, propulsion, and electrical submodels inside mission-analysis and sizing loops so that reported quantities correspond to a physically consistent operating point obtained by iterating across disciplines until mutual agreement is reached.

We implement these coupled analyses using the open-source Future Aircraft Sizing Tool with Overall Aircraft Design (FAST-OAD) [26], which we have extended with domain expertise and recent modules for hybrid-electric and distributed propulsion systems. FAST-OAD is built on the OpenMDAO infrastructure and follows a modular component paradigm: each discipline is encapsulated as a component, data transfers and solver couplings are made explicit, and the problem is defined by the set of design variables, constraints, driver(s), and chosen discipline submodels. This modularity makes the tool flexible in practice: it can run isolated single-point evaluations for sampling, execute nested solver sequences to obtain fully coupled convergence across subsystems, or serve as the computationally expensive black-box evaluator inside surrogate-assisted global optimization loops. Because individual discipline modules (geometry, aerodynamics, mass estimation, propulsion and power electronics, mission integration, electrical load-flow, etc.) can be replaced or enriched with user-provided submodels, the framework supports targeted fidelity control and straightforward incorporation of component-specific behavior across the design space.

Because the DRAGON test case exhibits strong nonlinear interactions between its aerodynamic, structural, and electrical subsystems, the standard fixed-point coupling between disciplines used in baseline FAST-OAD was adapted to better handle equilibrium between disciplines. This ensures that key feedback loops, such as those linking propulsion power, mass, and energy balance, converge more reliably under tight coupling conditions. Moreover, we use low-fidelity disciplines by relying on equation-based approximation or very coarse space discretizations. Still, a full multidisciplinary evaluation, including powertrain and load-flow analyses, sizing loops, and mission fuel computation, requires approximately 2 to 5 minutes per run on an Intel Core Ultra 9 185H vPro processor. Despite being much faster than high-fidelity disciplinary chains because of the many approximations the simulator relies on, this computational cost makes the MDA model effectively a nonlinear blackbox for large-scale optimization.

To overcome this, in the following, surrogate models are trained on FAST-OAD outputs to approximate the equilibrium solutions of the coupled disciplines efficiently. These metamodels accelerate global exploration and enable explainable-AI techniques to reveal key sensitivities and design drivers—while remaining grounded in the underlying multidisciplinary physics.

4.5 Surrogate modeling

The 1000 points suggested by the previously defined DoE have been evaluated through the simulator, yielding 1000 inputs and outputs. From that, two datasets of 300 and 700 couples are derived.

Concerning the metamodel, we employed the Kriging with Partial Least Squares (KPLS) with three latent variables, a squared exponential kernel for continuous variables, and a continuous relaxation kernel for categorical variables.

A KPLS surrogate model is then trained over the 300-point dataset. This surrogate leads to a relatively small RMSE of 1.42% over the other 700-point dataset, making our surrogate appropriate for proper knowledge extraction. Data are available online¹.

4.6 Explainable methods, analyses, and insights extraction

For this problem, we use SHAP and PDP complemented with ICE for explainability analysis. Global Sensitivity Analysis (GSA) using SHAP and PDP was also performed to investigate the influence of input variables on the output. One thing worth mentioning here is that the use of SHAP and PDP allows the quantification of the impact of categorical variables, which is not possible if we use variance-based decomposition methods. Based on the extension of KPLS to categorical variables in [87] and the extension of PDP, SHAP, and GSA to such variables in [83], we can represent the importance of the categorical variables, their coupling effects, and even their influence in the form of a boxplot.

4.6.1 Global sensitivity analysis

Global sensitivity analysis (GSA) identifies the fan overall pressure ratio (OPR) and the wing sweep angle as the most influential variables; their partial dependence and SHAP results are shown in Fig. 4 and Fig. 5, respectively. The four variables, horizontal-tail aspect ratio (HT AR), HT sweep angle, HT taper ratio (HT TR), and the sizing take-off field length (TOFL), contribute to less than 1% of the model's explained importance on the output and can therefore be considered effectively non-influential. Notably, the choice of electric architecture ranks comparably in importance to the initial climb slope angle and the wing aspect ratio. The turboshaft layout and wing taper ratio exhibit moderate effects,

¹https://github.com/ANR-MIMICO/SMPT_XAI

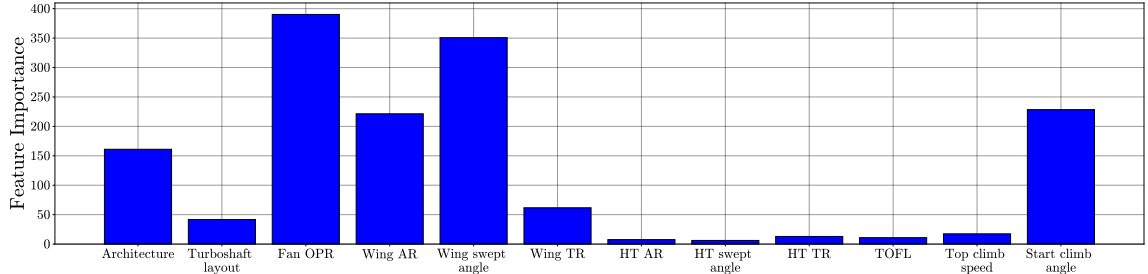


Fig. 4: GSA results from partial dependence functions for the DRAGON problem.

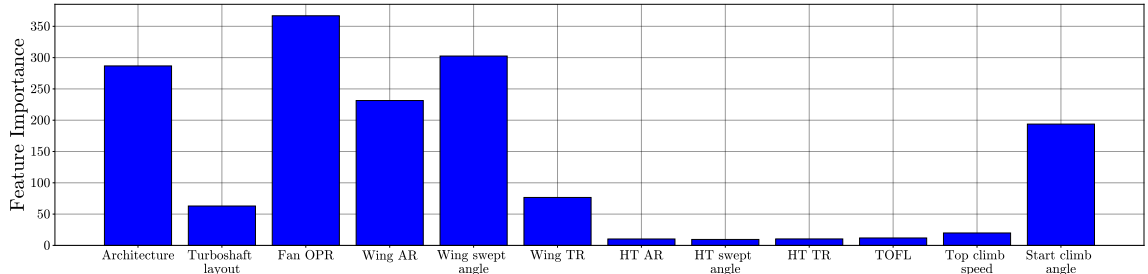


Fig. 5: GSA results from the averaged SHAP values for the DRAGON problem.

though their influence is smaller than that of the architecture choice. Because the underlying model is a fast equation-based proxy, the impact of turboshaft layout is likely underestimated; this moderate effect therefore advocates for follow-up studies with higher-fidelity models [48].

Clearly, the importance of categorical variables (primarily architecture) is notably higher when using averaged SHAP values compared to the partial dependence values. The difference arises from the way the importance of categorical variables is formulated in PDP (as shown in Eq. 4), which relies on heuristics and differs from the treatment of continuous variables. In contrast, SHAP applies the same equation for both categorical and continuous variables, ensuring a consistent approach across feature types. Given this consistency and the theoretical foundations of SHAP, it is generally better to trust the averaged SHAP values over PDP when assessing feature importance (especially when involving categorical variables), as they provide a more reliable and unified measure of an input’s contribution to the model’s predictions [64].

4.6.2 Local explainability visualization

The PDPs and SHAP dependence plots (Fig. 6 and Fig. 7) summarize each variable’s influence and help reveal interactions. For visualization, ICE curves are color-coded by Fan OPR (the most influential variable), except the Fan OPR plot itself, which is colored by wing swept angle; SHAP dependence points are colored by the secondary variable of interest. The wing swept angle exhibits a clear non-monotonic effect on fuel mass: fuel mass decreases with sweep up to about 30° and then increases beyond that. By contrast, several continuous variables show largely monotonic effects (*e.g.*, higher Fan OPR tends to increase fuel mass, while larger wing aspect ratio tends to decrease it), although some nonlinearities remain (for example, fuel mass rises increasingly steeply with higher start climb angles). PDPs for variables with negligible influence sometimes display both increasing and decreasing trends; these are likely surrogate artefacts and should not be overinterpreted.

Interactions are visible in both ICE and SHAP plots. For Fan OPR, the ICE curves show a stronger effect when the wing swept angle is small (steeper gradients), and conversely, the influence of the wing swept angle on fuel burn is amplified at high Fan OPR, therefore highlighting a bidirectional interaction. The start climb angle, wing aspect ratio, and other important variables similarly have larger effects when Fan OPR is high. For variables with minimal global influence (*e.g.*, HT-AR), apparent interactions with Fan OPR are unreliable and should be treated cautiously. SHAP dependence plots show the same interaction patterns, but they can be visually subtler; scattered SHAP values for dominant variables (wing swept angle, Fan OPR) nonetheless corroborate the presence of interactions.

The impact of categorical variables is worth looking at with SHAP, as outlined before, because it is more reliable than ICE in this setting. Using architecture 1 as the reference in Fig. 7, we observe that architecture 10 generally leads to a smaller fuel mass than the first architecture. On the other hand, some architectures (most notably, architectures 8 and 9) lead to higher fuel mass than the reference architecture. Therefore, ignoring the presence of constraints for now, architectures 10 and 15 seem to

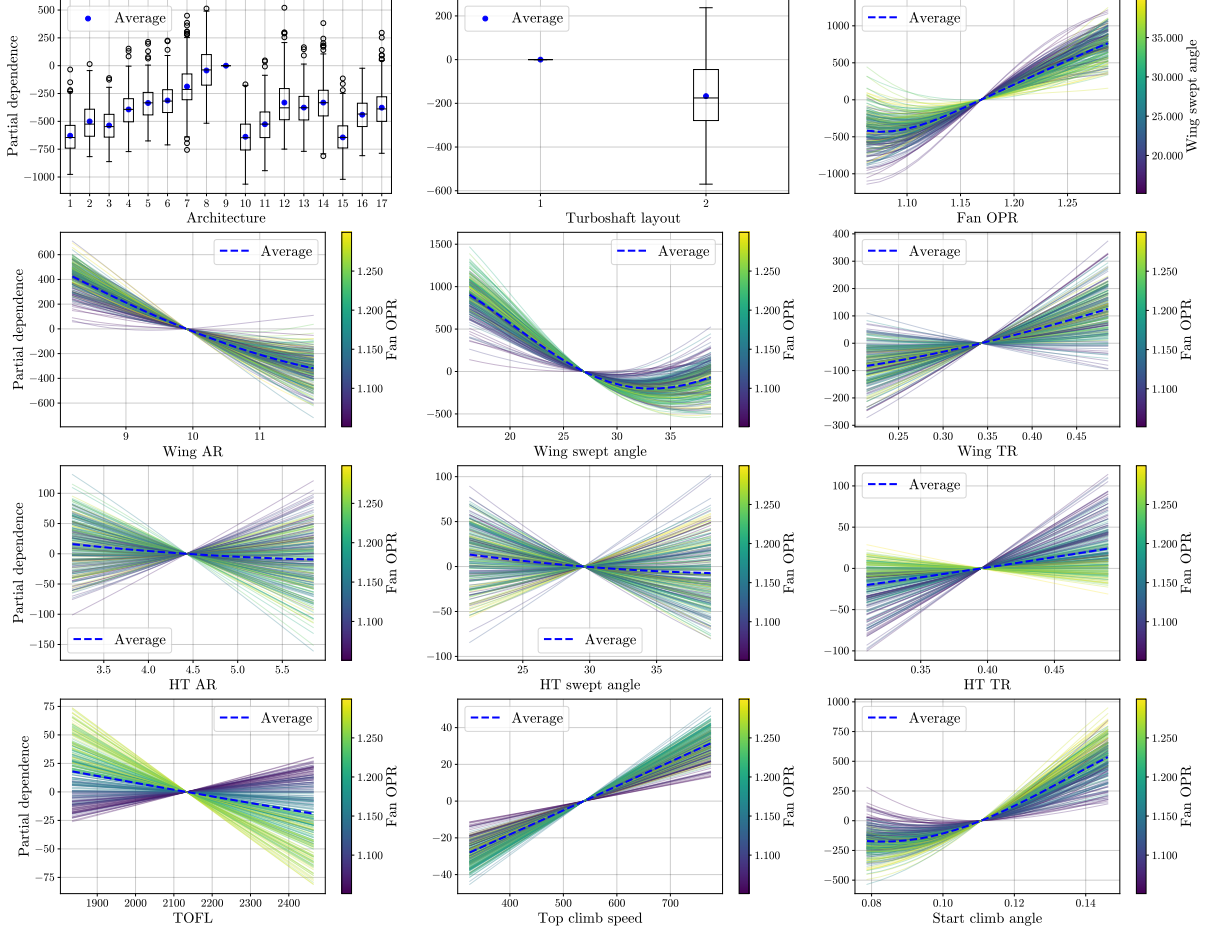


Fig. 6: PDP and ICE curves for the DRAGON problem.

be the best choice when the goal is to minimize fuel mass. Similarly, one can also see that the second turboshaft layout generally leads to reduced fuel mass compared to the first layout, although its impact on fuel mass is not as significant as the choice of architecture.

The SHAP summary plot, as shown in Fig. 8, gives a direct interpretation of all continuous variables at the same time. It is worth noting that it is not useful to include categorical variables in the SHAP dependence plot since there is no natural ordering of the categorical variables. Both PDP+ICE and SHAP generally provide similar insights. However, in our opinion, PDP+ICE offers a clearer view of how interactions with other variables influence the way a specific variable affects fuel mass. In this regard, PDP/ICE provides a faster and clearer intuition by showing direct relationships between input variables and the output. PDP alone is intuitive enough, but it does not supply information on the impact of interactions, which role is fulfilled by ICE.

Through our explainability analysis, we explored the impact of key design variables, such as electric generator sizing, battery energy density, distribution of fan thrust, and wing structural stiffness, on fuel mass. By integrating global sensitivity measures and local explainers, we revealed how multi-physics interactions drive design trade-offs, such as the non-linear coupling between electrical subsystem sizing and aerodynamic drag penalties. Hence, we transform FAST-OAD from a mere predictive tool into a transparent decision-support environment, enabling co-design across aerodynamicists, electrical engineers, structural analysts, and system architects to collaboratively refine the DRAGON architecture. This first demonstration provides a valuable test case to showcase how metamodels, when coupled with explainability techniques, can reveal the influence of design parameters on the objective of an engineering problem. In this context, it offers insights into how various aircraft parameters impact fuel consumption. When combined with previous optimization studies, this analysis not only validates the key drivers identified through optimization but also enhances understanding by highlighting why certain design choices lead to reduced fuel mass. Such explainability supports more informed decision-making in the early stages of aircraft design.

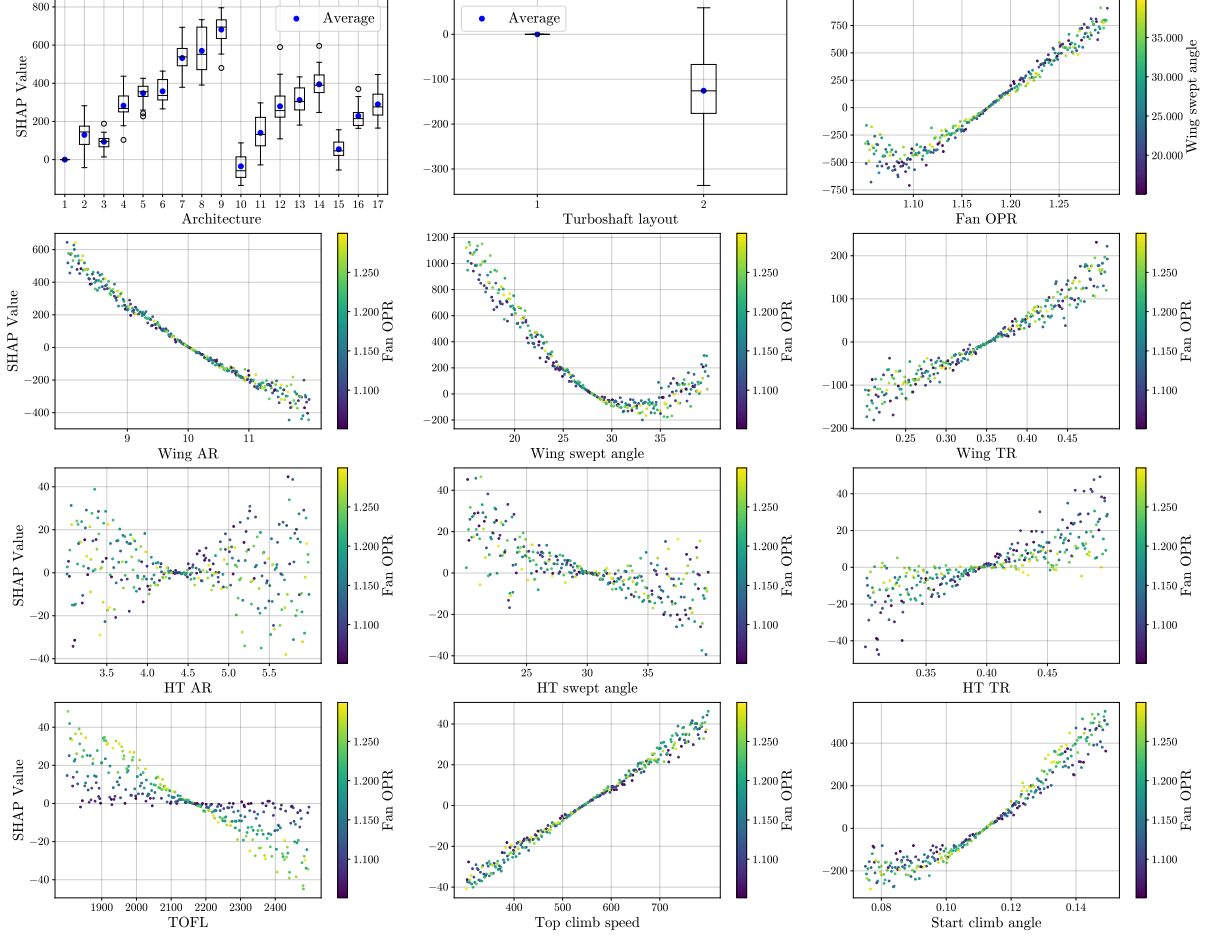


Fig. 7: SHAP dependence plot for the DRAGON problem.

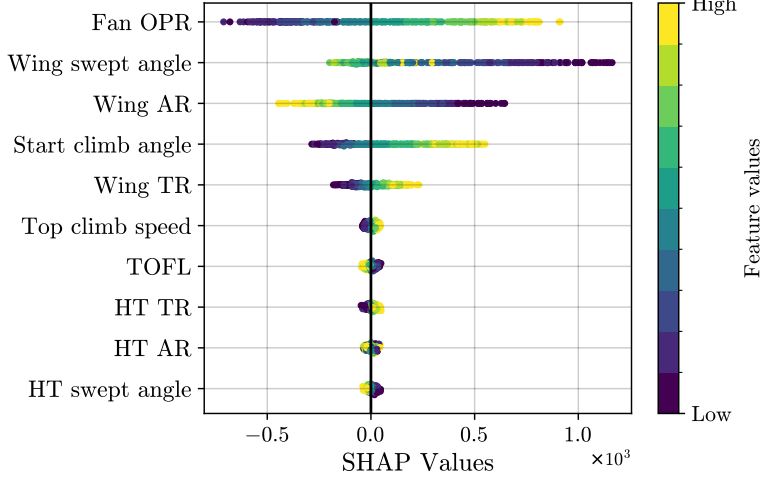


Fig. 8: SHAP beeswarm plot for the DRAGON problem continuous variables.

Surrogate models combined with XAI are highly useful for early-stage co-design: surrogates enable rapid exploration of large design spaces, while XAI reveals which inputs, interactions, and architecture choices most strongly influence performance and why. In the DRAGON framework, these insights are actionable: they guide architecture screening, prioritize optimization effort, and indicate where to raise discipline fidelity in FAST-OAD. To capture the stochastic and operational behaviors that static MDA and surrogate evaluations cannot represent, the next section introduces socio-technical dynamic simulations based on ABM. Integrating ABMs with our surrogate/XAI stack extends interpretability from

isolated, pointwise trade-offs to time-dependent, system-level dynamic behaviors, reveals emergent constraints driven by operational processes, and enables richer, context-aware design analysis. Accordingly, we conduct a second, more systematic case study that leverages XAI to quantify how dynamic operational behaviors alter earlier surrogate-based conclusions and to identify which feature attributions remain robust under surrogate model approximations and operational uncertainty.

5 Agent-based model exploration for decision support

Agent-Based Modeling (ABM) is a powerful tool for simulating complex systems based on autonomous agents that interact with one another and with their environment. These models are particularly important for studying emergent phenomena, for example, when local interactions give rise to global behaviors that are often difficult to capture with traditional analytical methods [27]. ABM provides a powerful framework for the emulation of complex systems made up of autonomous agents interacting in a dynamic environment, such as epidemiology, economics, or urban planning, offering a bottom-up approach to understand emergent phenomena [14, 34]. They are fundamentally stochastic to emulate the unknown individual behavior and to better capture the epistemic uncertainty over the underlying phenomena.

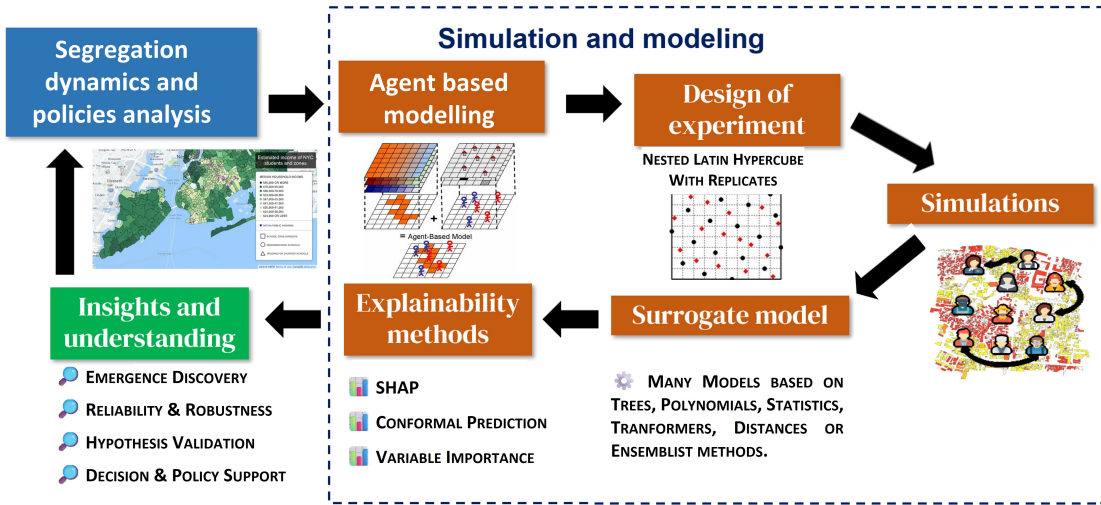


Fig. 9: Workflow for interpretable surrogate models for an analysis-oriented simulation.

Figure 9 illustrates our workflow for integrating interpretable surrogate models into an assessment-oriented simulation pipeline: this is an instance of the workflow already introduced in Fig. 1 but adapted to this agent-based problem. Our workflow starts with the definition of the ABM and the generation of a Design of Experiments over the input space of the Schelling segregation model parameters. Furthermore, each point in the DoE is evaluated through five independent replications to account for the stochastic variability inherent in socio-technical ABM simulations (*e.g.* to estimate pointwise mean and variance) [18]. The choice of five repetitions was driven by computational budget but could also be selected adaptively, driven by variance-based stopping rules using uncertainty-quantification or sequential design methods [71]. Each simulation is evaluated using a high-fidelity simulator to obtain two chosen target outputs. Various surrogate models are then trained and compared on this dataset to emulate the costly simulator with substantially reduced computational cost. Surrogates principally approximate the simulator's input-output mapping under uncertainty. Nevertheless, surrogate predictions and derived explanations remain approximations of the true simulator and must be validated accordingly. XAI techniques are applied to the surrogate models to quantify global and local input effects and to generate human-interpretable attributions that support the co-design process. Overall, the workflow supports four related objectives: (i) support decision and assess intervention impacts via systematic what-if exploration; (ii) improve model reliability and robustness through replication and sensitivity analysis; (iii) hypothesis testing and theory validation by linking micro-rules to macro-outcomes; and (iv) discovery of emergent behaviors that may affect policy choices. This section demonstrates the workflow on the Schelling model, extending our prior work [89] by adding an explicit uncertainty quantification study and a systematic

XAI comparison across surrogate families, moving towards robust, ensemble-based interpretation for uncertain Simulations of Agent-Based Model (SABM).

First, Section 5.1 introduces the social system of interest and describes its main territory characteristics and actionable design variables together with the equilibrium target. After that, the workflow unfolds as described in Fig. 9. Section 5.2 then describes the agent-based modeling approach for multi-agent systems handling; Section 5.3 introduces the Design of Experiments for the design space and the aggregated output metrics used to train surrogates; Section 5.4 details the simulator implementation and analyzes the generated dataset; Section 5.5 presents the surrogate models, and Section 5.6 reports the global and local XAI analyses, highlights key interactions and trade-offs.

5.1 Segregation dynamics

The residential segregation model introduced by *T. Schelling* investigates how individual local decisions can give rise to global segregation patterns [90]. It demonstrates that even agents with only mild preferences for neighbors of their own type, without any explicit intention to form homogeneous neighborhoods, can nonetheless produce highly segregated outcomes.

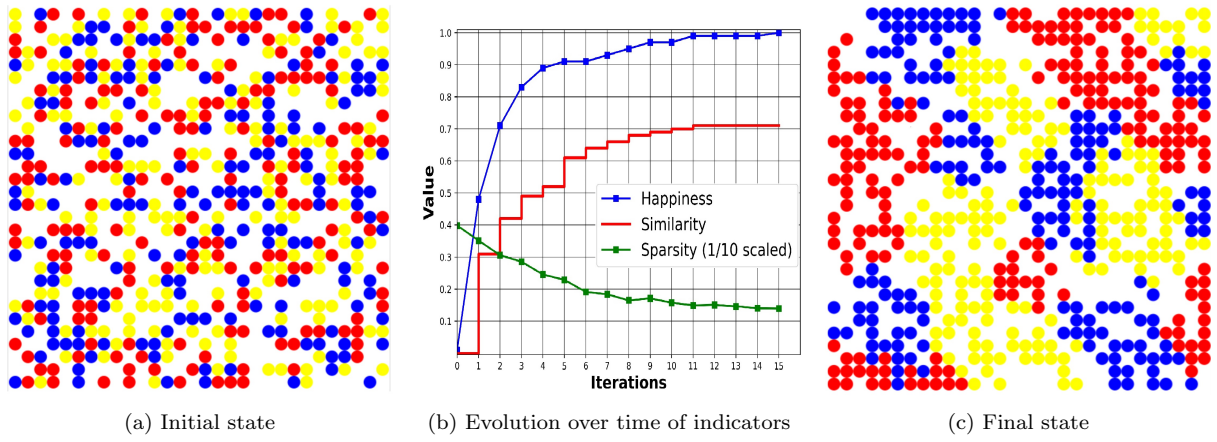


Fig. 10: An instance of the segregation problem simulated on the GAMA platform.

In our setting of the Schelling model, agents are randomly placed on a square lattice and assigned a *type* (visualized by color). An agent is **Happy** if the proportion of its *neighbors* that are of a different type is below its *intolerance threshold*; otherwise it is **Unhappy**. At each time step, all unhappy agents move to a randomly chosen empty cell, and the simulation stops when all agents are happy (an equilibrium is reached). Besides the intolerance threshold, three parameters govern agents' behavior: the agent's *perception distance* (neighborhood radius), the agent's *density* (fraction of occupied cells), and the square map's *edge length*. Finally, it is useful to distinguish *socially actionable* variables such as density, perception, or intolerance from *contextual* or structural variables such as the city size or its population diversity (number of types), since they have different implications for interpretation and intervention [89].

This problem involves five input variables, consisting of three continuous and two integer variables, which jointly determine the dynamics of the segregation model. The three continuous variables correspond to the population density, intolerance threshold, and perception distance, while the two integer variables specify the number of individual types and the grid size. These variables, summarized in Tab. 4, control both the structural configuration of the environment and the behavioral tendencies of agents, making them central to the analysis.

Function/Variable	Nature	Range
Number of individual types	int	[2, 5]
Density of individuals	cont	[0.01, 1]
Intolerance threshold	cont	[0, 1]
Size of the square grid edges	int	[10, 40]
Perception distance	cont	[1, 10]

Table 4: Design variables for diversity analysis.

5.2 Agent-based modeling

An Agent-Based Model (ABM) generally consists of *agents*, which operate according to predefined or adaptive behavioral rules; an *environment*, which structures spatial and network interactions; and *interaction mechanisms*, which govern the behavior of the agents and the evolution of the system [72]. Depending on their design, ABMs can be classified as *rule-based models* (following explicit logical instructions), *stochastic models* (incorporating probabilistic elements), or *hybrid models* (combining adaptive learning mechanisms). In practice, most multi-agent models are stochastic, as randomness is often introduced in agents' decision-making, initial conditions, or interaction patterns to reproduce realistic variability.

However, as the number of agents and interactions increases, the computational cost associated with ABMs grows rapidly, making large-scale simulations computationally intractable without important computational capacities [63]. Furthermore, their stochastic nature typically requires running many simulations to obtain statistically meaningful results, further amplifying the computational burden [34]. In addition, these models may require extensive parameter calibration, involving thousands of runs to achieve a reliable fit. Similarly, uncertainty quantification remains a challenge, as slight variations in input parameters can lead to significant discrepancies in outcomes.

ABM offers a natural multiscale framework for Schelling's segregation model or other related multi-agent systems: they explicitly encode heterogeneous agents, local interaction rules, and a spatially structured environment. In Schelling-type models, an agent follows a simple tolerance rule which, under repeated stochastic updates, can amplify mild individual preferences into pronounced macro-scale segregation [90]. This bottom-up perspective shows how network topology, update protocols, and randomness interact to produce phase transitions, path dependence, and multiple equilibria, making ABMs especially suited to study emergent, multi-scale phenomena under epistemic uncertainty.

5.3 Design of experiments and aggregated output metrics

In order to efficiently explore the parameter space, we generated a Design of Experiments (DoE) using nested Latin Hypercube Sampling (LHS), based on a uniform distribution [3]. We generated an LHS of 200 points, structured to include a subset of 50 points that preserves LHS. These nested LHS are generated with the ESE (Enhanced Stochastic Evolutionary algorithm) criterion as implemented in SMT (Surrogate Modeling Toolbox) [54]. The nested structure provides both uniform stratified coverages and separated training and validation subsets for robust performance assessment [21]. Furthermore, to account for the stochastic aspects, we repeated five times for every simulation parameter. This represents a total of $m = 1000$ simulations (200×5), the exact same number as in Section 4. We choose a training set of 25% and a validation set of 75% of the complete dataset to test whether learning on a small dataset can reproduce the analyses obtained from a more exhaustive exploration.

To validate our workflow for both regression and classification, we consider two types of outputs: a binary variable indicating convergence and a continuous variable representing sparsity [95].

A simulation is **convergent** if it stops because no individual moves on the grid anymore. However, knowing that a simulation may never converge, we set a threshold of 1000 iterations; after that, the simulation is stopped and considered **non-convergent**.

The ratio between the number of unlikely and likely neighbors is called the u/l measure. For an agent at cell coordinates (i, j) , its u/l ratio is given by:

$$[u/l]_{i,j} = \frac{q_{i,j} + w_{i,j}}{s_{i,j}} \quad (9)$$

where $s_{i,j}$, $q_{i,j}$, and $w_{i,j}$ denote, respectively, the number of similar neighbors, different neighbors, and vacant cells surrounding the agent, with the agent considered a neighbor of itself to avoid division by zero.

The **sparsity** $\langle [u/l] \rangle$ of the population is obtained by averaging the $[u/l]$ measure over all agents:

$$\langle [u/l] \rangle = \frac{1}{N} \sum_{(i,j) \in C} [u/l]_{i,j} \quad (10)$$

where N is the total number of agents whose associated cells form the set C . For a grid with side length c and a density ρ , $N = \lfloor \rho c^2 \rfloor$.

5.4 Implementation of the simulator

In terms of implementation, we use the segregation model available in the model library of the open-source GAMA platform [99]. Figure 10 illustrates a simulation example with three types of agents, a density of 60%, an intolerance threshold of 33%, a perception distance of 3 units, and a grid of 30×30 . Cells without agents remain empty, while agents are colored according to their type. On the left, the initial state is generated randomly, with an average percentage of individuals present in the agents' neighborhood, referred to as **similarity**, almost zero, and many agents are unhappy. Gradually, the rate of happy agents, who then cease moving, increases until a stable state is reached after 15 iterations. This stable state, depicted on the right map, corresponds to an average dissimilarity of 30%. The sparsity, which characterizes how dispersed the agents are, gradually decreases as the agents cluster together, eventually stabilizing around 1.4. This model is both simple enough to understand the marginal impact of every variable and complex enough to induce multi-scale emergent behaviors through tangled nonlinear dynamics.

As for the engineering MDA that was based on fast approximations, here, we use an approximation of the problem that does not represent the geographical data and relies on homogeneous agents. It should also be noted that there are exogenous sources of random uncertainty arising from the initial positions of individuals and their movements from one iteration to the next. Notably, a simulation may fail to converge for two reasons. First, the parameterization may rule out any theoretical equilibrium. Second, an equilibrium may exist but not be reached within the 1000 iterations: when agents move randomly, independently, and without memory, the system can oscillate or follow a locally non-monotonic trajectory, delaying convergence.

A simulation lasts from 3 seconds to 30 minutes on an Intel Core Ultra 9 185H vPro processor. Thus, the agent model can be considered as an expensive blackbox, which motivates the use of surrogate models in this context.

Dataset analysis

The 1000 points suggested by the previously defined DoE have been evaluated through the simulator, yielding 1000 inputs and outputs in the considered dataset.

Compared to the aircraft design study, we propose to add a first descriptive data analysis of the complete dataset, as illustrated in Fig. 11, where for each of the 5 variables, the sparsity values are plotted against the different variable values. Converged simulations are shown in green, while simulations that reached 1000 iterations are shown in red. The distribution of sparsity values is presented in the sixth figure as a boxplot.

A high value of sparsity indicates either a strong mixing of agents or many vacant cells, thus translating into low segregation and high spatial entropy. Conversely, low sparsity means that most agents are surrounded by similar neighbors, indicating high segregation and a more orderly spatial organization, which results in reduced entropy [95].

Out of 1000 simulations, 546 converged and ended with an average sparsity of 6.20 compared to 9.27 for the 454 non-convergent simulations. Note that out of the 200 experiments, 16 partially converge, depending on the randomness in the 5 repetitions.

5.5 Surrogate modeling

Many studies have already demonstrated the value of surrogate models for learning from SABM for response surface predictions [36, 66, 1]. We will test this approach on the Segregation model by learning a surrogate model using 50 out of the 200 points, each repeated 5 times. Then, we test and compare the predictions of many resulting surrogate models based on this dataset. In all experiments, we used each model's default hyperparameter settings unless explicitly stated otherwise. We want to predict two outputs and therefore, we build two surrogate models, one for each output, and we address two tasks: (i) a regression problem to predict sparsity indices, and (ii) a classification problem to predict simulator convergence. In both cases, the surrogate models are trained as interpolative models over fixed, known input bounds.

Regarding the models tested from SMT [88], the Gaussian Process (GP) uses a heteroscedastic noise automatically estimated based on the repeated experiments [3], a linear trend (ordinary kriging), a squared exponential correlation kernel for regression, and an absolute exponential one for classification. Similarly, Radial Basis Functions (RBF) use a linear trend, and the Inverse Distance Weighting (IDW) interpolation method employs a squared exponential kernel for regression and an absolute exponential kernel for classification. For the Linear Regression (LR) and Quadratic Polynomial (QP) models, we use

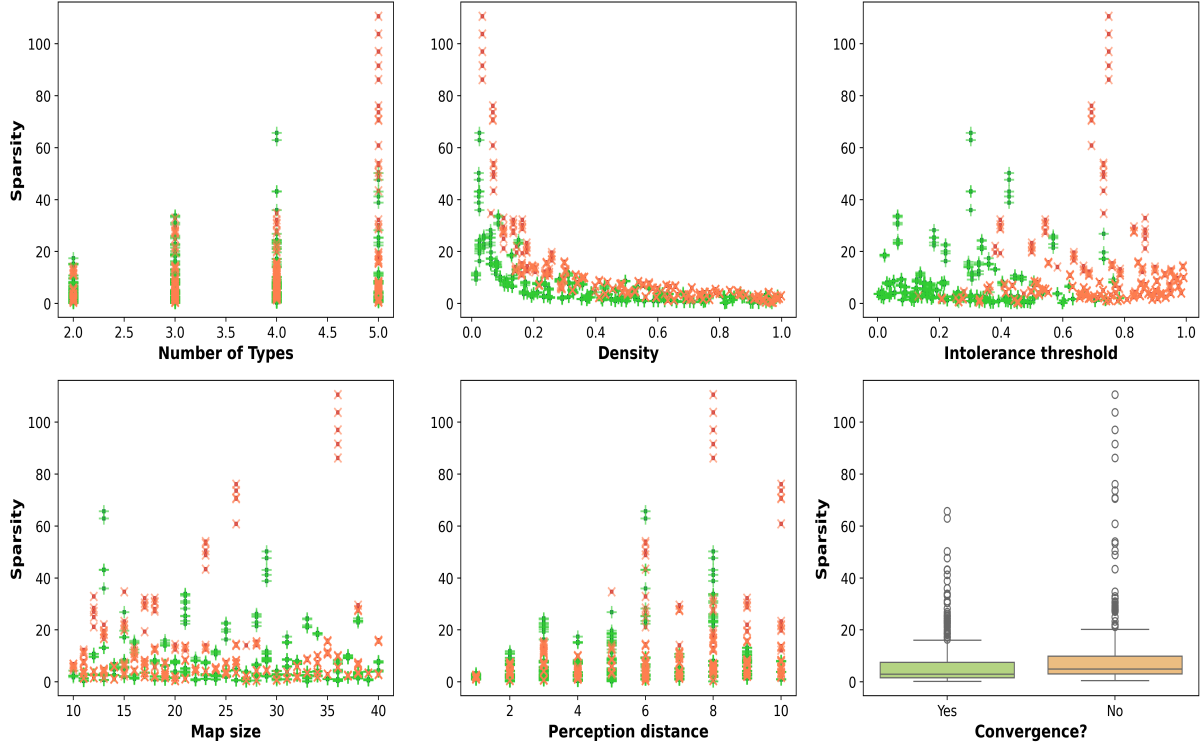


Fig. 11: The dataset with converged simulations in green and the others in red.

the default options, and for the Regularized Minimal-energy Tensor-product Splines (RMTS), we use the formulation based on Hermite cubic splines. Finally, for the Gradient-Enhanced Neural Network (GENN) model, we exploit the derivatives predicted by the GP, thereby enriching the information used during the network training. We also compare these models with methods from Scikit-learn [77]. Thus, for both regression and classification, we notably use the Decision Tree (DT), Random Forest (RF), k-Nearest Neighbors (kNN), MultiLayer Perceptron (MLP), as well as the Support Vector Machine (SVM). For the kNN method, we chose to use 15 neighbors, corresponding to 3 different locations, due to the repetitions. All these methods are implemented in two versions: a regression version to predict sparsity and a classification version to predict whether the ABM converges. As with Scikit-learn, the Gradient Boosting (GB) from the XGBoost library treats regression and classification separately [22]. We used the Polynomial Chaos Expansion (PCE) from OpenTurns [12] with default options. We use the foundation model Tabular Prior-Data Fitted Network (TabPFN) from PriorLabs [50]. To finish with, we use the Contextual Interactive Ensemble Learning (CIEL) framework developed at IRIT [13, 65], using its default sub-models: logistic regression for regression tasks and support-vector machines for classification. CIEL embeds simple learners in a cooperative multi-agent ensemble that handles nonlinearity via local cooperation and dynamically reweights sub-models by contextual meta-features to improve robustness and interpretability.

To validate our 16 surrogate models, we held out 150 input configurations (750 new observations) that were not used during training. We evaluate regression accuracy by the RMSE on this complete test set [4] and classification performance by the MCC, which balances true and false positives and negatives, and is especially informative under class imbalance and appropriate for the 2-class problem [23].

For the sparsity regression problem, we further assess uncertainty quantification via the PVA metric [53, 10] that assesses the adequacy of predicted variances by comparing them to the actual squared errors. A PVA value close to zero indicates that the predicted variances align well with the observed errors. For GP, we use the posterior variance directly, for RF, we rely on the sample variance across trees, and for TabPFN, we approximate variance from the interquartile range (0.15865, 0.84135) under a normal distribution assumption. All other models uncertainty quantification is based on a 50/50 split conformal prediction to estimate $\hat{\sigma}_i^2$ [91].

Note that our metrics are partial and subject to misinterpretation. For instance, the RMSE is an aggregated measure resuming average error and neither the maximal nor the median error, as such it gives little information on the error distributions, same for MCC which is less representative than the complete 4 values representing the confusion matrices or PVA which is based on a normal error

assumption and on the idea that the predicted variance should be equal to the unknown error. We use RMSE to have an idea of the global regression precision of the model, MCC because it is a symmetric metric to quantify the confusion matrices, and PVA because it consists of a simple metric that does not require any quantile computations. All results (RMSE, MCC and PVA) for the 16 surrogate models are reported in Tab. 5, where we have organized the models into the following categories: tree-based models (RF, GB, DT); kernel-based models (GP, RBF, SVM); linear and quadratic models (LR, QP); reduced basis models (RMTS, PCE); neighborhood-based models (kNN, IDW, CIEL); neural network models (MLP, GENN); and the transformer-based model (TabPFN). These various families are colored accordingly for more visibility, and the overall global aggregated results are in darker green when they have the best performances.

Model	RMSE	MCC	PVA	Reg. Rank	Class. Rank	PVA Rank
RF	6.86	0.83	4.13	3	4	11
GB	9.21	0.82	3.44	9	5	10
DT	8.34	0.75	4.19	7	8	12
GP	8.22	0.87	3.14	6	1	9
RBF	8.17	0.87	5.32	5	1	14
SVM	11.53	0.21	1.01	14	16	7
LR	8.56	0.82	0.24	8	6	1
QP	6.35	0.77	0.51	2	7	5
PCE	7.84	0.74	9.12	4	9	15
RMTS	11.60	0.52	9.98	15	11	16
kNN	11.75	0.30	0.40	16	15	3
IDW	10.57	0.41	4.62	11	13	13
CIEL	11.03	0.38	2.65	13	14	8
MLP	9.87	0.73	0.60	10	10	6
GENN	10.93	0.48	0.25	12	12	2
TabPFN	4.31	0.86	0.47	1	3	4

Table 5: Global predictive qualities comparison across 16 surrogate models, with darker green shades representing better performances.

Our results confirm that different surrogate models exhibit variable and complementary performances at the global scale, making them versatile and indicating promising future research towards a mixture of experts or ensemble approaches to combine various models. In particular, no method stands out as one of the top three for every metric, and no method falls into the bottom 4 for every metric.

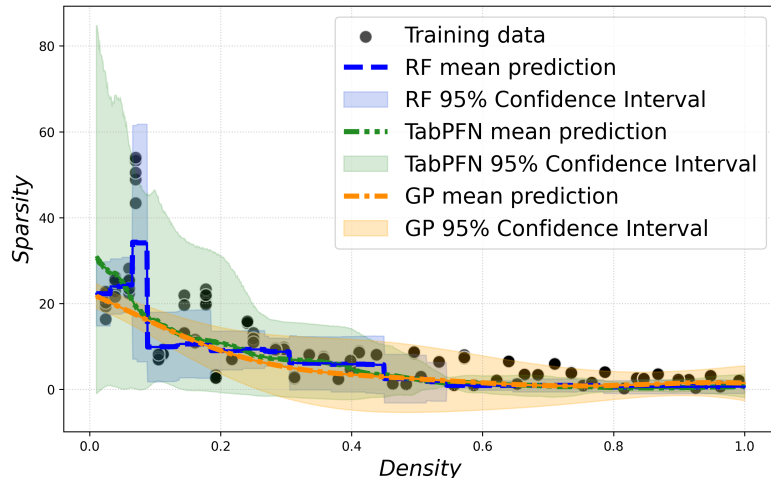


Fig. 12: RF, TabPFN, and GP response surfaces of sparsity as a function of density with the other variables fixed.

Ensemble methods have the disadvantage of requiring a large number of predictions to estimate uncertainties, thereby generating very discontinuous response surfaces, which can, in turn, limit their

analytical capacity, interpretability, and gradient prediction, but they open up many avenues for research. However, and quite surprisingly, LR and its slightly more complex counterpart QP perform quite well on this problem, even if they are simple polynomials of degree 1 and 2, respectively. Even if the latter behavior is hard to extrapolate to other problems, we argue that looking at and explaining the relationship of degree 1 or 2 is always good, as most global information is generally captured in such simple models, which can help detect relevant features really fast. Similarly, logic explanations such as abductive and contrastive explanations are known to be easy to compute based on a decision tree surrogate without any loss of generality [8]. Therefore, and even if RF and GP/RBF can outperform, respectively QP or DT we always recommend starting with these elemental, transparent surrogate models as they are the most efficient for a quick and first overview [49].

For the classification of convergent simulations, the RBF and GP models yielded the lowest misclassification rates with identical confusion matrices, followed closely by TabPFN and RF. LR and GB performed comparably: LR achieved more true positives (520 vs. 508) at the expense of fewer true negatives (389 vs. 402), but these compensating shifts led to nearly identical MCC values. Thus, despite different confusion-matrix profiles, LR and GB exhibit equivalent overall correlation between predicted and actual labels. These results highlight the strength of kernel and probabilistic models in learning decision boundaries under limited data. In contrast, SVM, IDW, CIEL, and kNN showed a high number of misclassifications, suggesting that distance-based classifiers struggle with the repeated simulations and sparse grid structure, although the weighting helps IDW to perform slightly better. LR, GENN, and kNN yielded PVA values close to zero. We obtained different aggregated metrics for different surrogate models, but to go further, we need to complement these global metrics with local analysis.

To also study the local predictions, let's examine more in-depth the qualitative behaviors of the three models that come with in-house uncertainty quantification. To do that, a spatial study comparing TabPFN, GP, and RF is provided in Fig. 12. In what follows, each variable has been fixed to its average value (or its integer part in the case of discrete variables) except for density, which varies between 0 and 1, to illustrate the smooth aspect of the GP and the TabPFN model and the piecewise continuous aspect of the RF along with the poor uncertainty estimation associated with it, obtained by resampling over 100 estimators (default options), whereas the GP can be directly used for variance-based interpretability [53]. TabPFN variance is obtained with its quantile prediction and shows a clear non-smooth and non-interpretable behavior. In fact, TabPFN overall variance prediction has been shown to overestimate the uncertainty when computing the PVA, whereas the GP tends more to underestimate it, in particular here with repeated experiences and aleatoric intrinsic noise to model. This one-dimensional example illustrates the complementarity of predictive models and the importance of adapting the model to the studied scale at hand. Therefore, the figure shows that two models can agree on the expected mean prediction but still predict very different standard deviations, highlighting the complementarity of global and local analyses. The TabPFN model is really time-consuming in inference, but still achieved the lowest RMSE and second best in classification error, indicating superior ability to capture the nonlinear mapping from input parameters to sparsity, as is also the case for RF and GP, which are well fitted for these low-data contexts. In fact, for this type of sparse and uniformly distributed data, it is generally preferable to use a GP or an RBF, as these models learn quickly and effectively capture nonlinear behaviors on small datasets [35]. Also, RF, as an ensemble approach, provides comparable results here, which can be explained by its ability to approximately reproduce the behaviors of nonlinear SABM. Gradient boosting and decision tree, coming slightly behind, also confirm the capacity of these methods to handle complex interactions among agents [95]. However, these results should be put in light of the approximation of such variance by conformal prediction, which is generally non-smooth. TabPFN's variance approximation via interquartile range also performed reasonably, whereas both GP and RF tend to underestimate the error because of repeated experiences.

5.6 Explainable methods, analyses, and insights extraction

The goal of this section is to leverage surrogate models for extracting insights on the underlying model by leveraging XAI methods.

5.6.1 Global sensitivity analysis

We aim to quantify how input parameters drive model outputs by applying multiple global sensitivity methods and checking the consistency of their conclusions. Global sensitivity analysis identifies influential inputs, dominant interactions, and how input uncertainty propagates to output variability. Although decision trees are limited and discontinuous, they are sequences of simple procedures that are easy to

interpret. For example, the first node of the GB or DT is “intolerance threshold below 0.63”, which confirms what was graphically observed on the complete dataset. In a random forest, the importance of a variable is often measured via the Mean Decrease in Impurity (MDI). At each split of a tree, the reduction in impurity, often measured by the Gini index, quantifies the probability that a sample is misclassified. This reduction is attributed to the variable that enabled the split, and by summing these reductions over all trees, a global measure of the importance of each feature is obtained. However, this approach can bias the estimation in favor of variables with high cardinality, which offer more splitting possibilities. In this way, in our test case, we obtain the importances shown in Fig. 13. For both outputs, the variables that most influence the model’s predictions, as identified on the extended dataset, are clearly found to be intolerance for convergence and density for sparsity. It is also observed that grid size has a rather weak influence on the outputs. Equivalent importance analyses can also be performed with other models. For instance, applying the same procedure to a k-nearest neighbors model and aggregating SHAP absolute values produces the results shown in Fig. 14. The predicted importances differ significantly from those of the random forest analysis, as most variables appear significant. This occurs because kNN SHAP values primarily reflect local, instance-specific effects rather than global trends, making them less suitable for traditional global sensitivity analysis. Appendix A further illustrates that importance outcomes vary depending on whether the surrogate captures broad system-level tendencies or local deviations, and as such, the SHAP importance of a Gaussian process is aligned with the random forest results of Fig. 14.

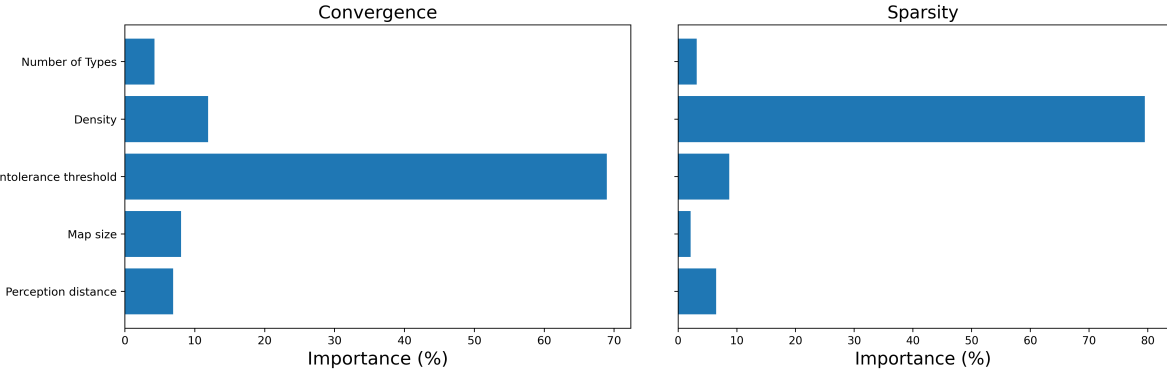


Fig. 13: Variables importance in the random forest based on MDI.

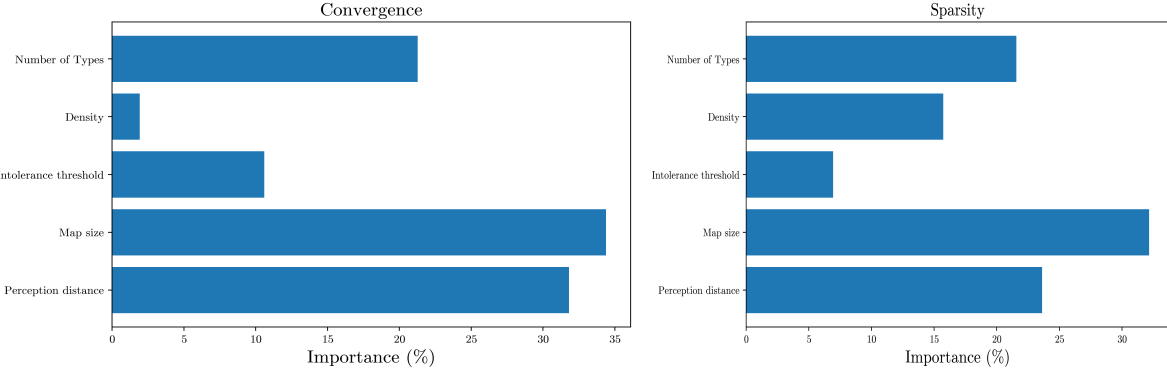


Fig. 14: Variables importance in the k-Nearest Neighbors based on SHAP.

5.6.2 Local explainability visualization

In addition, SHAP values provide a fine-grained local interpretation by quantifying the contribution of each variable to the prediction [93]. Thus, while MDI offers a global importance based on the sum of impurity reductions, SHAP values reveal how each feature locally influences the model’s output, enabling a more robust and nuanced analysis of the predictions. The SHAP values are calculated from the model’s predictions on the 1000-point dataset and plotted in Fig. 15. Note that, given the very low computational cost of surrogate models, they are fast to evaluate. SHAP values precisely assess the contribution of

each parameter and the distribution of these contributions. For example, we observe that intolerance and density have a major impact, which translates into significant variations in convergence or spatial structure. Thus, SHAP analysis complements the global interpretation provided by the random forest by showing locally how each parameter influences the prediction. For instance, the analysis reveals that the intolerance threshold has an extremely strong explanatory power, relatively centered and symmetric regarding the simulation's convergence. In contrast, for low density values, sparsity tends to explode and to overwhelm the other variables, revealing a more localized interpretability of density on sparsity.

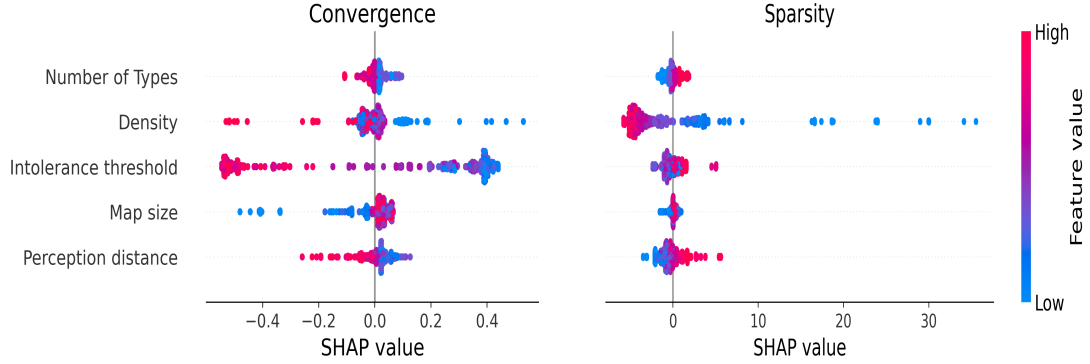


Fig. 15: SHAP values predicted by the random forest.

5.6.3 Comparing Instance-Level Explanations Across Multiple Surrogate Models

To quantify the quality of the explanations, we compute NDCG over each model's SHAP-value importance ranking in both the regression and classification tasks [15]. Note that these importance values are limited to their absolute influence and that other metrics taking into account the sign of the influence, such as the Composition of Rank, Influence, and Accuracy described in [103], may lead to different results. Fig. 16 displays, for both Convergence classification and Sparsity predictions, the NDCG adequacy of every pair of models in terms of SHAP values importance prediction on the validation test dataset. These SHAP prediction analyses reveal two subgroups of models whose diagonal elements belong to the subgroups with important internal NDCG scores and lower intergroup relationships, highlighting two groups of surrogate models sharing similar SHAP-based feature importance patterns, seemingly the local and the global models.

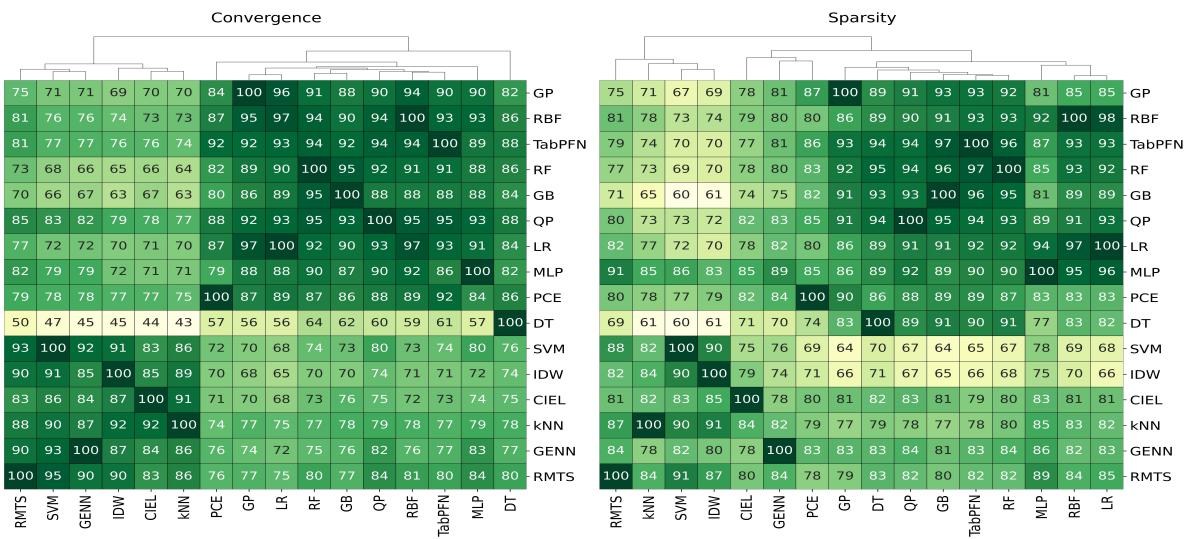


Fig. 16: SHAP values NDCG (%) for every pairs of clustered models.

To have more information on this subject, we show a deeper analysis based on a clustering algorithm that gives the dendrogram in Fig. 17. The dendrogram is obtained by agglomerative hierarchical clustering

(Lance-Williams) using the average-linkage criterion on the dissimilarity matrix based on the pairwise NDCG similarities. The latter produces a linkage matrix whose entries record the clusters merged, the distances, and the new cluster size, which can then be transformed into the dendrogram shown [24]. The dendrogram confirms the presence of two distinct groups, consistent with the separation observed in the NDCG matrices, as more than half of the total dissimilarity is accounted for by the first major branching (from approximately 1.3 to 0.6 on the dissimilarity scale). A first group containing models like GP and RBF that indeed appear in the same leaf as the first generalizes the second, followed by the similar models QP and LR, and to finish with, TabPFN seems to behave similarly to RF when it comes to generating SHAP explanations. In the second group, we have all other methods; indeed, GB and DT are in the same group, and in fact, DT gives the worst results on convergence prediction, being divergent in behavior, its ability to classify being really poor except with the GB methods, as the latter utilize DT as its core mechanism. We also have a subgroup with methods based on neighborhood, such as CIEL or kNN, which are closely related and, knowing their locality, would be more fit for LIME explanation. This is particularly true for local or linear-based models, including SVM or LR. Note that LIME is free to evaluate with a local linear predictor as in CIEL. In this second group, we also find IDW, the last local model, but also the two closely related neural networks (MLP and GENN) and the two last other nonlinear models based on spline and on polynomial, which are both smooth combinations of a few basis elements.

The first group, in orange, contains the algorithms most prone to over-specialization, which tend to excel on familiar scenarios but struggle to generalize to broader, unseen patterns. Conversely, the second group, in green, contains models most prone to overfitting when they become too complex, all of which capture noise rather than general patterns. These findings suggest that, in most cases, our explanations characterize the surrogate rather than the underlying Schelling model we intended to understand.

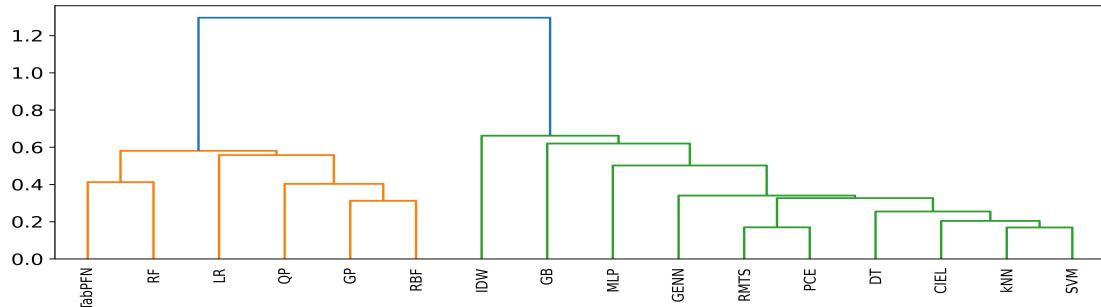


Fig. 17: SHAP values NDCG based hierarchical clustering.

An additional local analysis using SHAP and PDP is given in Appendix A. It inspects model-wise SHAP values and model agreement/disagreement to assess variable importance and explanation reliability, confirming that some models capture global trends while local effects appear as noise, whereas others recover local tendencies but overfit. While SHAP and PDP were primary, alternatives (Sobol' indices [83], HSIC [53], conformal prediction [83], LIME [13]) are applicable. Overall, surrogate models provide meaningful explanations for SABM even with sparse data.

Overall, TabPFN, RF, and GP strike the best balance between accuracy, uncertainty quantification, and interpretability. Kernel methods (RBF) excel in classification, whereas ensemble and Bayesian approaches provide reliable uncertainty estimates. Models with poor regression fit (*e.g.* kNN or IDW) also yield low explanation fidelity, underscoring the link between predictive performance and interpretability. However, the most striking result is that RF, GN, DT, or QP, even if really simple models, could yield highly reliable results, and this seems to confirm their use in practice [31].

These findings offer practical guidance for selecting surrogate models in SABM, depending on whether regression precision, classification reliability, uncertainty calibration, or interpretable explanations are the primary objectives. Future work should explore benchmark problems with analytically known mechanisms (*e.g.* Lotka-Volterra/SIR dynamics) to further validate and compare SHAP-based explanation methods in this context [36, 91] and discuss many other types of explanations beyond SHAP [51]. Still, these results thus provide a solid foundation for model selection depending on the targeted applications.

These findings support recent advances in the use of surrogate models for SABM, which not only accelerate computations but also provide crucial uncertainty estimates for interpreting emergent phenomena in complex systems [36].

6 Conclusions and perspectives

This work set out to demonstrate how surrogate modeling combined with explainable AI (XAI) can turn computationally expensive, blackbox simulators into interpretable, trustworthy tools for decision support. By deliberately exploring two complementary domains, a Multidisciplinary Design Analysis and Optimization (MDAO) engineering test case and an Agent-Based Model (ABM) for socio-technical policy assessment, we show how the same workflow addresses distinct modeling challenges.

The MDAO case highlights the strengths of surrogate models in structured, high-dimensional design spaces where the main bottleneck is the cost of high-fidelity solvers. In this context, surrogates act as accelerators: they reproduce key performance metrics of the aircraft-design problem at a small fraction of the computational cost, enabling rapid trade-off exploration and optimization. XAI techniques further illuminate which design variables drive critical outputs, supporting engineering intuition, sensitivity analysis, and clearer communication across design teams.

By contrast, the ABM case exposes domains dominated by uncertainty, stochasticity, and emergent behavior. Socio-technical simulations, such as segregation models, are better viewed as computational laboratories for testing interventions and assessing robustness under variability rather than deterministic performance curves. Here, surrogates do more than speed up computation: they enable systematic replication, variance decomposition, and exploration of policy scenarios that would otherwise be prohibitive. XAI complements this by mapping model assumptions and input distributions to emergent collective outcomes, bridging the gap between technical modeling and stakeholder understanding.

Seen together, the two cases illustrate complementary facets of a surrogate-driven XAI workflow. The MDAO setting emphasises precision, smooth response surface methodologies, and exploration of high-dimensional multimodal design spaces; the ABM setting emphasizes stochastic exploration, robustness, and interpretation of emergent phenomena. Both converge on the methodological insight that surrogates and XAI are enablers, rather than end goals, of transparent, efficient simulation science: they make computer experiments into a usable numerical laboratory.

Methodologically, our experiments indicate several practical recommendations. Careful diagnostic-driven workflows that combine space-filling and adaptive sampling, probabilistic and ensemble surrogates, and complementary explainability tools provide a practical path to both accelerate and interpret complex simulations. Ensemble approaches are often particularly valuable because model diversity helps capture different aspects of the underlying simulator at both global and local scales. For stochastic simulators, repeated sampling and ensembles help capture intrinsic variability and avoid misleading point estimates. However, two research questions remain to be addressed more thoroughly: (i) How should surrogate choice and explainability methods be matched to specific interpretive goals and scales? (ii) How can these methodological components be integrated into a recommendation system that automates surrogate and XAI selection for simulation-based design?

We also identify important limitations and caveats. Explicit uncertainty accounting, systematic validation, and transparent reporting are necessary if surrogate–XAI pipelines are to be reliable components of engineering and policy co-design. Validating the original simulator can be difficult when the “ground truth” is unknown or when outputs are aggregated and may hide emergent behaviors. The surrogate introduces a further layer of approximation: assessing its predictive fidelity and uncertainty requires independent validation, replication to capture stochastic variability, and attention to both error metrics and uncertainty quality. More notably, the surrogate-based explanations characterize the surrogate rather than the complex system. Finally, mixed variable types (discrete choices, architectural options, continuous sizing parameters) demand surrogate and XAI methods that can handle heterogeneous inputs without losing interpretability. Building on this, future studies will address the integration of both adaptive sampling and XAI within our unified workflow that can be applied to a broad range of simulation models.

By training lightweight emulators on a relatively small number of simulations, we obtained order-of-magnitude speedups while reproducing key behaviors. In the DRAGON electric-hybrid aircraft design study, a surrogate trained on about 300 configurations recovered critical trade-offs between sizing parameters, identified dominant variables, and revealed interaction patterns that otherwise would have required hundreds of costly CFD and structural runs. In the urban segregation agent-based model, a surrogate trained on roughly 50 stochastic realizations reproduced segregation indices and spatial patterns, and

SHAP-based explanations highlighted policy levers (for example, population density and perceived neighborhood diversity) that influence sparsity and segregation outcomes. Across both studies, we validated surrogates not only on predictive accuracy but also on their ability to explain global trends and local variabilities.

Practically, combining space-filling and adaptive sampling, probabilistic and ensemble surrogates, and XAI tools yields a workflow that accelerates exploration of expensive simulators, provides traceable input–output links, supports human-in-the-loop what-if analysis, and reduces computational cost by focusing simulations on the most informative regions. Ensemble approaches are especially useful because model diversity helps capture different aspects of the simulator at both global and local scales, and repeated sampling is important for stochastic systems to avoid misleading point estimates.

Trustworthy use of surrogate–XAI pipelines requires explicit attention to evaluation. Original simulators can be hard to validate when ground truth is unknown or when outputs are aggregated and may mask emergent behaviors; calibration and verification are necessary but not always sufficient. Surrogates introduce approximation error, so assessing predictive fidelity and uncertainty needs independent validation, replication to capture stochastic variability, and metrics that quantify both pointwise accuracy and uncertainty quality. Mixed variable types (discrete architectural choices, categorical socio-types, continuous sizing parameters) demand surrogate and XAI methods that handle heterogeneous inputs without losing interpretability. In conclusion, augmenting surrogate models with explainability transforms expensive simulators into interpretable, interactive decision tools that support robust design under uncertainty and human-centered co-design. Making explainability a core design principle rather than a post-hoc add-on helps balance predictive fidelity with the clarity needed for collaborative decision processes.

Looking ahead, several directions can increase robustness and practical value. Multi-fidelity and hybrid approaches that combine coarse and fine models can reduce costs while preserving accuracy. Sequential and adaptive active learning schemes, such as multi-objective Bayesian optimization, can progressively enrich datasets and focus computing on informative regions for exploration, rare-event estimation, or reliability assessment. Embedding causal reasoning and counterfactual explanations could make recommendations more actionable under uncertainty. Improving the handling of mixed variables and spatio-temporal data will help surrogates and XAI scale to heterogeneous inputs and dynamic systems. Finally, real-time integration of surrogate-based XAI loops in participatory platforms can enable continuous stakeholder engagement, rapid iteration, and transparent decision-making by integrating visual interfaces to transparently communicate predictions, uncertainty, and explanatory insights.

Conflict of interest

The authors have no conflict of interest to declare.

Data availability and replication

The codes and data used to produce the results are open-source and available online: https://github.com/ANR-MIMICO/SMPT_XAI.

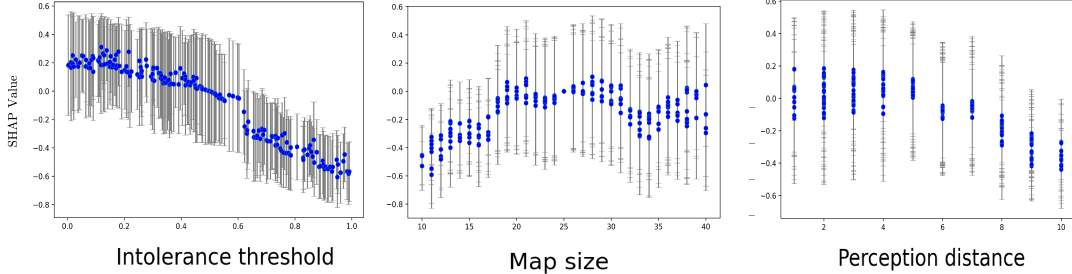
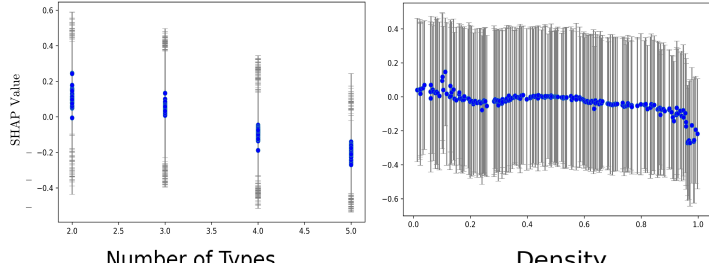
Acknowledgements

Pramudita Satria Palar would like to acknowledge financial support from Institut Teknologi Bandung through the Riset Kolaborasi Internasional 2025 scheme. This work is part of the activities of ONERA - ISAE - ENAC joint research group. The research presented in this paper has been performed in the framework of the MIMICO research project funded by the Agence Nationale de la Recherche (ANR) n° ANR-24-CE23-0380.

A Complementary Local Analysis of Variable Importance

To complement the pairwise agreement analysis of Section 5.6, Fig. 18 shows the mean SHAP values as a function of input variables, with uncertainty represented as agreement \pm disagreement across the 120 model pairings. Together, these analyses provide both a global perspective via pairwise and clustered agreement, and a local view through variable-level SHAP behavior. The latter enables a more complete interpretability assessment across surrogate model families.

Convergence



Sparsity

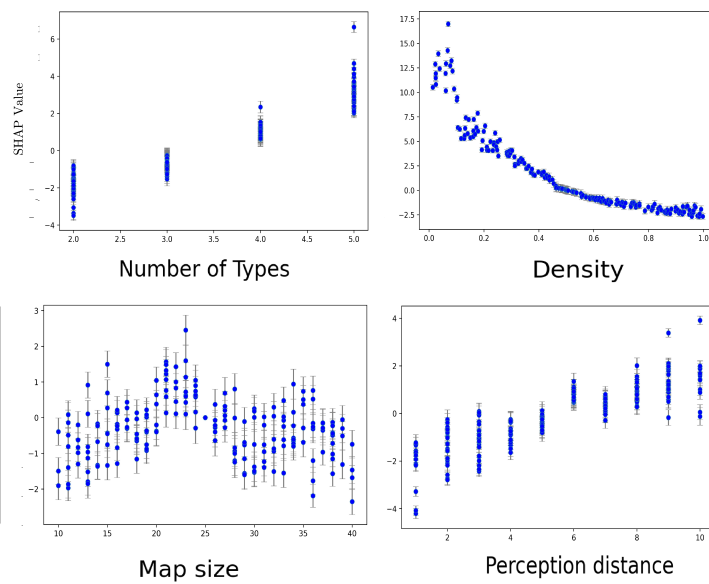


Fig. 18: SHAP values as a function of the variables predicted by the average of all surrogate models.

Figure 18 shows an aggregated visualization of all the models, but the explanations could also be drawn model-wise, generating the two groups identified in the dendrogram of Fig. 17. These plots emphasize which regions in the input space yield robust explanations and where model disagreement suggests higher epistemic uncertainty. For instance, in low-density data regions, SHAP values tend to fluctuate more across models, reflecting instability in the learned attributions. Conversely, high-agreement regions highlight stable model behavior and consistent variable influence, supporting model trust. The models in the orange group predict a high influence for intolerance on convergence and for density on sparsity, which are the most prominent average effects, whereas the models in the green group give more importance to the local effect even if not significant in average, such as density on convergence and map size on sparsity which explains the two groups disagreeing on the variable importance as shown in the NDCG matrices of Fig. 16.

All features being treated equally, SHAP mainly helps identify which features influence the similarity measure most. Comparing SHAP values across models offers valuable insights into feature importance and model behavior (highlighting consistency, model-specific priorities, and robustness checks) yet requires caution because SHAP ranges and meanings differ by algorithm. While such comparisons can inform feature selection and deepen understanding, they don't directly indicate which model is superior.

In conclusion, SHAP values help explain model predictions, but their interpretation differs depending on the algorithm. Orange models, such as GP, reflect how each feature affects the predicted mean and uncertainty of the output, and SHAP highlights feature importance in shaping the underlying function rather than direct instance similarity. On the contrary, green models such as kNN make predictions based on the similarity between data points, using distances in feature space. SHAP values here indicate how much each feature contributes to determining the nearest neighbors and shaping the final prediction. There is no clear response on what is a “really important” variable, except that it depends on whether the interest of the practitioner is more in the global trends or in the potential local effects. Moreover, studying a complex system through a surrogate model is a strongly impacting method to gather information, as most of the resulting information comes from the structure of the surrogate model itself instead of coming from the complex system.

In Fig. 19, the Partial Dependence Plots (PDP) illustrate the average effect of each variable on the prediction by neutralizing the influence of the others, while the Individual Conditional Expectation (ICE) curves reveal the variability of individual responses, highlighting the interactions between the parameters [73] predicted on the validation set by the GP surrogate model.

In the presented figure, the global trends observed in the PDP/ICE, such as a monotonic or non-linear effect on the output, are confirmed by the dispersion of the SHAP values, which also reveals the presence of interactions, although these are relatively weak for some parameters. These complementary analyses thus provide a deep and nuanced understanding of the model’s behavior and the influence of each variable on the simulation. The PDPs show the average effect of each variable on the predicted outputs by neutralizing the influence of the other parameters. This allows us to determine whether the effect of a variable is monotonic, such as increased density making convergence more difficult, or if there is a non-linear relationship, such as an optimum or a tipping point. The ICE curves reveal the prediction trajectories for each individual simulation. If these deviate significantly from the PDP curve, it highlights interactions between the studied variable and other variables or random factors: for instance, the intolerance threshold may increase or decrease sparsity depending on the perception distance and whether the simulation converges or not, leading to a non-representative PDP average.

Convergence

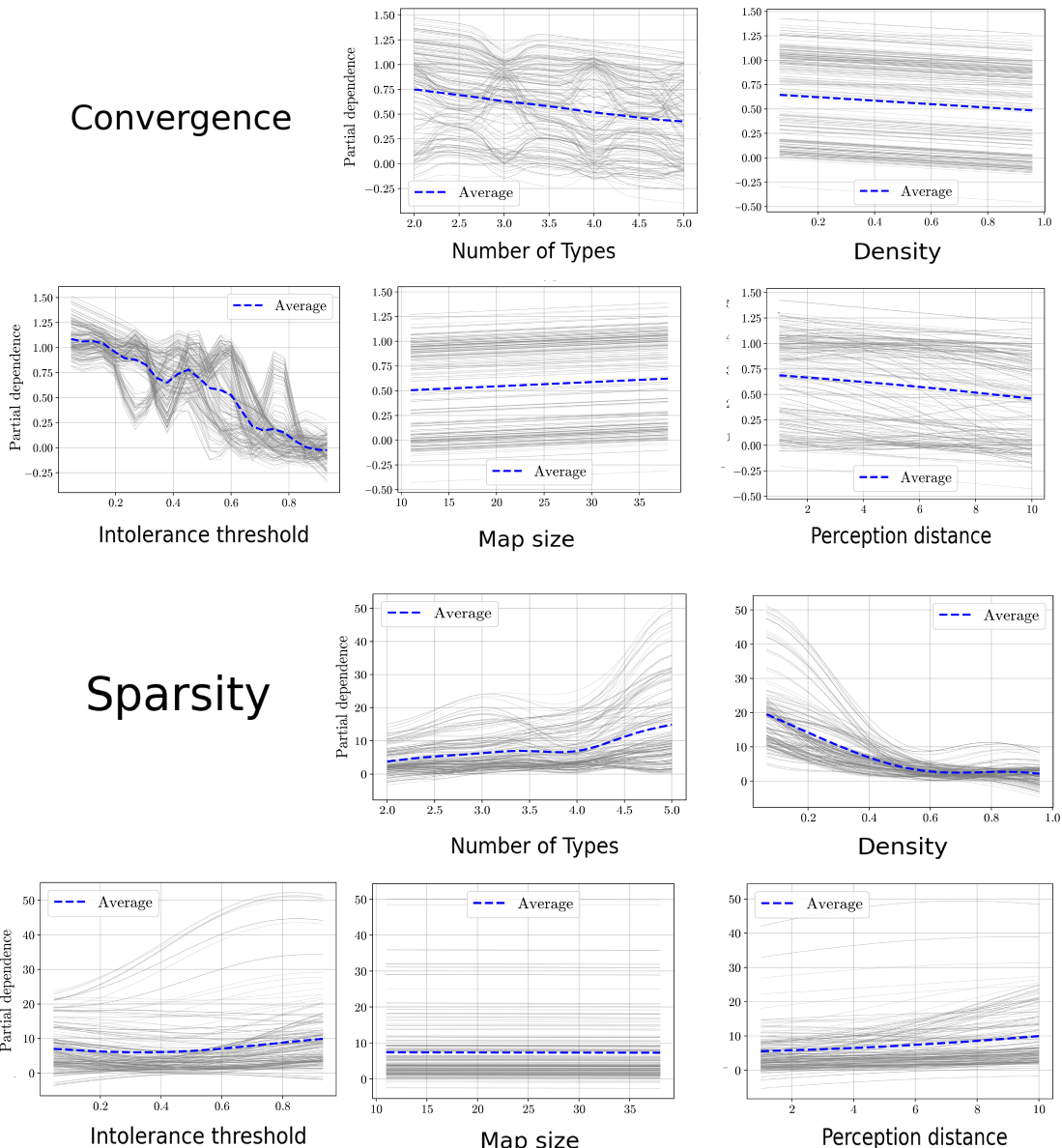


Fig. 19: PDP and ICE plots as a function of the variables predicted by the GP model.

References

- [1] Claudio Angione, Eric Silverman, and Elisabeth Yaneske. Using machine learning as a surrogate model for agent-based simulations. *Plos one*, 17(2), 2022.
- [2] Daniel Apley and Jingyu Zhu. Visualizing the effects of predictor variables in black box supervised learning models. *Journal of the Royal Statistical Society Series B: Statistical Methodology*, 82(4):1059–1086, 2020.
- [3] Rubén Conde Arenzana, Andrés López-Lopera, Sylvain Mouton, Nathalie Bartoli, and Thierry Lefebvre. Multi-fidelity gaussian process model for CFD and wind tunnel data fusion. In *AeroBest 2021*, pages 12–23, 2021.
- [4] Scott Armstrong and Fred Collopy. Error measures for generalizing about forecasting methods: Empirical comparisons. *International journal of forecasting*, 8(1):69–80, 1992.
- [5] Zenith Arnejo, Benoit Gaudou, Mehdi Saqalli, and Nathaniel Bantayan. Automatic generation of abm narratives using simulation traces and llm. In *The 26th International Workshop on Multi-Agent-Based Simulation*, 2025.
- [6] Zenith Arnejo, Benoit Gaudou, Mehdi Saqalli, and Nathaniel Bantayan. Communicating agent-based models to stakeholders: A scoping review. *Journal of Artificial Societies and Social*

Simulation, 28(2), 2025.

- [7] Antonin Arsac, Gabriel Sarazin, Aurore Lomet, and Jean-Philippe Poli. Fast hsic-based tests for random processes. In *International Conference on Industrial, Engineering and Other Applications of Applied Intelligent Systems*, pages 392–404. Springer, 2025.
- [8] Gilles Audemard, Steve Bellart, Louenou Bounia, Frédéric Koriche, Jean-Marie Lagniez, and Pierre Marquis. On the explanatory power of boolean decision trees. *Data & Knowledge Engineering*, 142:102088, 2022.
- [9] Charles Audet and Warren Hare. *Introduction: tools and challenges in derivative-free and blackbox optimization*. Springer, 2017.
- [10] François Bachoc. Cross validation and maximum likelihood estimations of hyper-parameters of Gaussian processes with model misspecification. *Computational Statistics & Data Analysis*, 66:55–69, 2013.
- [11] Adama Barry, François Bachoc, Sarah Bouquet, Miguel Zuniga, and Clémentine Prieur. Optimal design of physical and numerical experiments for computer code calibration. *arXiv preprint*, 2024.
- [12] Michaël Baudin, Anne Dutfoy, Bertrand Iooss, and Anne-Laure Popelin. Openturns: An industrial software for uncertainty quantification in simulation. In *Handbook of uncertainty quantification*, pages 2001–2038. Springer, 2017.
- [13] Clément Blanco-Volle, Nicolas Verstaevel, Stéphanie Combettes, Marie-Pierre Gleizes, and Michel Povlovsich Seixas. Explainability and interpretability of an ensemble multi-agent system for supervised learning. In *PRIMA 2024*, pages 335–350, 2024.
- [14] Jörg Bremer and Sebastian Lehnhoff. Decentralized coalition formation in agent-based smart grid applications. In *PAAMS 2016*, pages 343–355, 2016.
- [15] Chris Burges, Tal Shaked, Erin Renshaw, Ari Lazier, Matt Deeds, Nicole Hamilton, and Greg Hullender. Learning to rank using gradient descent. In *Proceedings of the 22nd international conference on Machine learning*, pages 89–96, 2005.
- [16] Jasper Bussemaker, Paul Saves, Nathalie Bartoli, Thierry Lefebvre, and Rémi Lafage. System architecture optimization strategies: dealing with expensive hierarchical problems. *Journal of Global Optimization*, 91(4):851–895, 2025.
- [17] Jasper Bussemaker, Paul Saves, Nathalie Bartoli, Thierry Lefebvre, and Björn Nagel. Surrogate-based optimization of system architectures subject to hidden constraints. In *Proceedings of the AIAA Aviation Forum*, page 4401, 2024.
- [18] Álvaro Carmona-Cabrero, Rafael Muñoz-Carpena, Woi Sok Oh, and Rachata Muneepeerakul. Decomposing variance decomposition for stochastic models: Application to a proof-of-concept human migration agent-based model. *Journal of Artificial Societies and Social Simulation*, 27(1), 2024.
- [19] Anouck Chan, Anthony Fernandes Pires, Thomas Polacsek, Stéphanie Roussel, François Bouissière, Claude Cuiller, and Pierre-Eric Dereux. Goal modelling in aeronautics: Practical applications for aircraft and manufacturing designs. *Data & Knowledge Engineering*, 155:102375, 2025.
- [20] Anouck Chan and Thomas Polacsek. Stroke management: Defining and assigning goals to stakeholders. In *42nd International Conference on Conceptual Modeling*, 2023.
- [21] Rémy Charayron, Thierry Lefebvre, Nathalie Bartoli, and Joseph Morlier. Towards a multi-fidelity & multi-objective Bayesian optimization efficient algorithm. *Aerospace Science and technology*, 142:108673, 2023.
- [22] Tianqi Chen and Carlos Guestrin. XGBoost: A Scalable Tree Boosting System. In *Proceedings of the 22nd ACM SIGKDD International Conference on Knowledge Discovery and Data Mining*, pages 785–794, 2016.
- [23] Davide Chicco, Valery Starovoitov, and Giuseppe Jurman. The benefits of the Matthews correlation coefficient (MCC) over the diagnostic odds ratio (DOR) in binary classification assessment. *Ieee Access*, 9:47112–47124, 2021.
- [24] Richard Cormack. A review of classification. *Journal of the Royal Statistical Society: Series A (General)*, 134(3):321–353, 1971.
- [25] Elisa Cueille, Déborah Bodini, Benoit Gaudou, Delphine Grancher, Pierre Nicolle, Olivier Payrastre, Manon Prédhumeau, Isabelle Ruin, Galateia Terti, and Nicolas Verstaevel. Assessing the impact of crisis cell decisions during flash flood. In *The 26th International Workshop on Multi-Agent-Based Simulation*, 2025.
- [26] Christophe David, Scott Delbecq, Sébastien Defoort, Peter Schmollgruber, Emmanuel Benard, and Valerie Pommier-Budinger. From FAST to FAST-OAD: An open source framework for rapid overall aircraft design. In *IOP Conference Series: Materials Science and Engineering*, volume 1024, page

012062. IOP Publishing, 2021.
- [27] Benjamin De Bosscher, Seyed Ziabari, and Alexei Sharpanskykh. Towards a better understanding of agent-based airport terminal operations using surrogate modeling. In *MABS 2023: Multi-Agent-Based Simulation Workshop*, pages 16–29, 2023.
 - [28] Benyamin De Leeuw, Seyed Ziabari, and Alexei Sharpanskykh. Surrogate modeling of agent-based airport terminal operations. In *International Workshop on Multi-Agent Systems and Agent-Based Simulation*, pages 82–94. Springer, 2022.
 - [29] Julien Demange-Chryst, François Bachoc, and Jérôme Morio. Shapley effect estimation in reliability-oriented sensitivity analysis with correlated inputs by importance sampling. *International Journal for Uncertainty Quantification*, 13(3), 2023.
 - [30] Michel dos Santos Soares and Jos Vrancken. Model-driven user requirements specification using SysML. *Journal of Software*, 3(6):57–68, 2008.
 - [31] Filip Došilović, Mario Brčić, and Nikica Hlupić. Explainable artificial intelligence: A survey. In *2018 41st International convention on information and communication technology, electronics and microelectronics*, pages 0210–0215. IEEE, 2018.
 - [32] Alexis Drogoul, Diane Vanbergue, and Thomas Meurisse. Multi-agent based simulation: Where are the agents? In *International Workshop on Multi-Agent Systems and Agent-Based Simulation*, pages 1–15. Springer, 2002.
 - [33] Vincent Dubourg, Bruno Sudret, and Jean-Marc Bourinet. Reliability-based design optimization using Kriging surrogates and subset simulation. *Structural and Multidisciplinary Optimization*, 44:673–690, 2011.
 - [34] Michael Dunne, Hossein Mohammadi, Peter Challenor, Rita Borgo, Thibaud Porphyre, Ian Vernon, Elif Firat, Cagatay Turkay, Thomas Torsney-Weir, Michael Goldstein, Hui Reeve, Richard Fang, and Ben Swallow. Complex model calibration through emulation, a worked example for a stochastic epidemic model. *Epidemics*, 39:100574, 2022.
 - [35] Joel Dyer, Patrick Cannon, Doyne Farmer, and Sebastian Schmon. Black-box Bayesian inference for agent-based models. *Journal of Economic Dynamics and Control*, 161:104827, 2024.
 - [36] Gianluca Fabiani, Nikolaos Evangelou, Tianqi Cui, Juan Bello-Rivas, Cristina Martin-Linares, Constantinos Siettos, and Ioannis Kevrekidis. Task-oriented machine learning surrogates for tipping points of agent-based models. *Nature communications*, 15(1):4117, 2024.
 - [37] William Fauriat. *Un discours de la méthode au XXI^e siècle: Risques et limites de l'intelligence artificielle*. Librinova, France, mar 2022.
 - [38] Luis Fonseca, Lucas Böttcher, Borna Mehrad, and Reinhard Laubenbacher. Optimal control of agent-based models via surrogate modeling. *PLOS Computational Biology*, 21(1), 2025.
 - [39] Mahmoud Fouda, Eytan Adler, Jasper Bussemaker, Joaquim Martins, Dilek Kurtulus, Luca Boggero, and Björn Nagel. Automated hybrid propulsion model construction for conceptual aircraft design and optimization. In *33rd Congress of the International Council of the Aeronautical Sciences, ICAS 2022*, 2022.
 - [40] Jerome Friedman. Greedy function approximation: a gradient boosting machine. *Annals of statistics*, pages 1189–1232, 2001.
 - [41] Moncef Garouani, Adeel Ahmad, Mourad Bouneffa, Mohamed Hamlich, Gregory Bourguin, and Arnaud Lewandowski. Towards big industrial data mining through explainable automated machine learning. *The International Journal of Advanced Manufacturing Technology*, 120(1–2):1169–1188, 2022.
 - [42] Moncef Garouani, Ayah Barhrhouj, and Olivier Teste. Xstacking: An effective and inherently explainable framework for stacked ensemble learning. *Information Fusion*, page 103358, 2025.
 - [43] Moncef Garouani and Mourad Bouneffa. *Unlocking the Black Box: Towards Interactive Explainable Automated Machine Learning*, page 458–469. Springer Nature Switzerland, 2023.
 - [44] Moncef Garouani, Josiane Mothe, Ayah Barhrhouj, and Julien Aligon. Investigating the duality of interpretability and explainability in machine learning. In *36th International Conference on Tools with Artificial Intelligence*, pages 861–867, 2024.
 - [45] Konstantinos Gavriilidis, Andrea Munafo, Wei Pang, and Helen Hastie. A surrogate model framework for explainable autonomous behaviour. *arXiv preprint*, 2023.
 - [46] Alex Goldstein, Adam Kapelner, Justin Bleich, and Emil Pitkin. Peeking inside the black box: Visualizing statistical learning with plots of individual conditional expectation. *Journal of Computational and Graphical Statistics*, 24(1):44–65, 2015.
 - [47] Justin Gray, John Hwang, Joaquim Martins, Kenneth Moore, and Bret Naylor. OpenMDAO: an open-source framework for multidisciplinary design, analysis, and optimization. *Structural and*

Multidisciplinary Optimization, 59(4):1075–1104, 2019.

- [48] Anaïs Luisa Habermann, Moritz Kolb, Philipp Maas, Hagen Kellermann, Carsten Rischmüller, Fabian Peter, and Arne Seitz. Study of a regional turboprop aircraft with electrically assisted turboshaft. *Aerospace*, 10(6):529, 2023.
- [49] Roel Henckaerts, Katrien Antonio, and Marie-Pier Côté. When stakes are high: Balancing accuracy and transparency with model-agnostic interpretable data-driven surrogates. *Expert Systems with Applications*, 202:117230, 2022.
- [50] Noah Hollmann, Samuel Müller, Lennart Purucker, Arjun Krishnakumar, Max Körfer, Shi Hoo, Robin Schirrmeister, and Frank Hutter. Accurate predictions on small data with a tabular foundation model. *Nature*, 637(8045):319–326, 2025.
- [51] Linwei Hu, Jie Chen, Vijayan N Nair, and Agus Sudjianto. Surrogate locally-interpretable models with supervised machine learning algorithms. *arXiv preprint*, 2020.
- [52] Marouane Il Idrissi, Vincent Chabridon, and Bertrand Iooss. Developments and applications of Shapley effects to reliability-oriented sensitivity analysis with correlated inputs. *Environmental Modelling & Software*, 143:105115, 2021.
- [53] Bertrand Iooss, Vincent Chabridon, and Vincent Thouvenot. Variance-based importance measures for machine learning model interpretability. In *Maîtrise des Risques et de la Sécurité de Fonctionnement*, pages 120–135. Springer, 2022.
- [54] Ruichen Jin, Wei Chen, and Agus Sudjianto. An efficient algorithm for constructing optimal design of computer experiments. *Journal of Statistical Planning and Inference*, 134(1):268–287, 2005.
- [55] Antoine Joulia, Judicaël Bedouet, Claire Sarrat, Céline Parzani, and Thomas Dubot. First steps towards aviation climate impact assessment using ATMLab. In *Towards Sustainable Aviation Summit*, 2025.
- [56] Cheikhou Kane, Samba Diaw, Mandicou Ba, Alassane Bah, and Etienne Delay. EcoSysML: A metamodel for socio-ecological systems (ses) integrating machine learning. In *Intelligent Systems Conference*, pages 24–40. Springer, 2025.
- [57] Navroop Kaur and Harjot Kaur. A multi-agent based evacuation planning for disaster management: a narrative review. *Archives of Computational Methods in Engineering*, 29(6):4085–4113, 2022.
- [58] Marc Kennedy and Anthony O'Hagan. Bayesian calibration of computer models. *Journal of the Royal Statistical Society: Series B (Statistical Methodology)*, 63(3):425–464, 2001.
- [59] Patrick Knab, Sascha Marton, Udo Schlegel, and Christian Bartelt. Which LIME should I trust? concepts, challenges, and solutions. *arXiv preprint*, 2025.
- [60] Andrew Lambe and Joaquim Martins. Extensions to the design structure matrix for the description of multidisciplinary design, analysis, and optimization processes. *Structural and Multidisciplinary Optimization*, 46(2):273–284, 2012.
- [61] Guerlain Lambert, Céline Helbert, and Claire Lauvernet. Quantization-based latin hypercube sampling for dependent inputs with an application to sensitivity analysis of environmental models. *Applied Stochastic Models in Business and Industry*, 41(3):e2899, 2025.
- [62] Pierre L'Ecuyer and Christiane Lemieux. Variance reduction via lattice rules. *Management Science*, 46(9):1214–1235, 2000.
- [63] Ju-Sung Lee, Tatiana Filatova, Arika Ligmann-Zielinska, Behrooz Hassani-Mahmooei, Forrest Stonedahl, Iris Lorscheid, Alexey Voinov, Polhill Gareth, Zhanli Sun, and Dawn Parker. The complexities of agent-based modeling output analysis. *Journal of Artificial Societies and Social Simulation*, 18(4), 2015.
- [64] Yong-Geon Lee, Jae-Young Oh, Dongsung Kim, and Gibak Kim. Shap value-based feature importance analysis for short-term load forecasting. *Journal of Electrical Engineering & Technology*, 18(1):579–588, 2023.
- [65] Jordan Levy, Clément Blanco-Volle, Nicolas Verstaevle, Benoit Gaudou, and Vincent Talon. Time-CIEL: contextual interactive ensemble learning for time series classification. In *23rd International Conference on Practical applications of Agents and Multi-Agent Systems (PAAMS 2025)*, 2025.
- [66] Barbara Llacay and Gilbert Peffer. Categorical surrogation of agent-based models: A comparative study of machine learning classifiers. *Expert Systems*, 42(1):e12987, 2025.
- [67] Scott Lundberg and Su-In Lee. A unified approach to interpreting model predictions. In *Advances in Neural Information Processing Systems*, volume 30, pages 4765–4774, 2017.
- [68] Charles Macal and Michael North. Tutorial on agent-based modeling and simulation. In *Proceedings of the Winter Simulation Conference, 2005*. IEEE, 2005.
- [69] Andreas Madsen, Himabindu Lakkaraju, Siva Reddy, and Sarath Chandar. Interpretability needs a new paradigm. *arXiv preprint*, 2024.

- [70] Joaquim Martins. Aerodynamic design optimization: Challenges and perspectives. *Computers & Fluids*, 239:105391, 2022.
- [71] Morgane Menz, Sylvain Dubreuil, Jérôme Morio, Christian Gogu, Nathalie Bartoli, and Marie Chiron. Variance based sensitivity analysis for Monte Carlo and importance sampling reliability assessment with Gaussian processes. *Structural Safety*, 93:102116, 2021.
- [72] Fabien Michel, Jacques Ferber, and Alexis Drogoul. Multi-agent systems and simulation: A survey from the agent community's perspective. In *Multi-Agent Systems*, pages 3–25. CRC Press, 2018.
- [73] Christoph Molnar. *Interpretable Machine Learning*. Lulu.com, 2019.
- [74] Pramudita Palar, Yohanes Bimo Dwianto, Lavi Zuhal, Joseph Morlier, Koji Shimoyama, and Shigeru Obayashi. Multi-objective design space exploration using explainable surrogate models. *Structural and Multidisciplinary Optimization*, 67(3):38, 2024.
- [75] Pramudita Palar, Lavi Zuhal, and Koji Shimoyama. Enhancing the explainability of regression-based polynomial chaos expansion by Shapley additive explanations. *Reliability Engineering & System Safety*, 232:109045, 2023.
- [76] Raghu Pasupathy and Kalyani Nagaraj. Modeling dependence in simulation input: The case for copulas. In *2015 Winter Simulation Conference (WSC)*, pages 1850–1864. IEEE, 2015.
- [77] Fabian Pedregosa, Gaël Varoquaux, Alexandre Gramfort, Vincent Michel, Bertrand Thirion, Olivier Grisel, Mathieu Blondel, Peter Prettenhofer, Ron Weiss, Vincent Dubourg, Jake Vanderplas, Alexandre Passos, David Cournapeau, Matthieu Brucher, Matthieu Perrot, and Édouard Duchesnay. Scikit-learn: Machine learning in Python. *Journal of Machine Learning Research*, 12(85):2825–2830, 2011.
- [78] Sébastien Petit, Julien Bect, Paul Feliot, and Emmanuel Vazquez. Parameter selection in Gaussian process interpolation: an empirical study of selection criteria. *SIAM/ASA Journal on Uncertainty Quantification*, 11(4):1308–1328, 2023.
- [79] David Planas Andrés, Eric Nguyen Van, Carsten Döll, and Philippe Pastor. Multi-disciplinary optimization of a distributed electric propulsion aircraft under aero-propulsive effects. *CEAS Aeronautical Journal*, 16(2):571–589, 2025.
- [80] Frank Ramsey. Truth and probability. In *Readings in formal epistemology: Sourcebook*, pages 21–45. Springer, 1926.
- [81] Suryateja Ravutla, Andrew Bai, Matthew Realff, and Fani Boukouvala. Effects of surrogate hybridization and adaptive sampling for simulation-based optimization. *Industrial & Engineering Chemistry Research*, 64(18):9228–9251, 2025.
- [82] Michael Ridel, Eric Nguyen Van, Tatiana Prosvirnova, David Donjat, Christel Seguin, and Philippe Choy. DRAGON: hybrid electrical architecture for distributed fans propulsion. In *MEA 2021*, 2021.
- [83] Mohammad Robani, Pramudita Palar, Lavi Zuhal, Paul Saves, and Joseph Morlier. Smt-ex: An explainable surrogate modeling toolbox for mixed-variables design exploration. In *Proceedings of the AIAA SciTech Forum*, Orlando, FL, USA, January 2025. American Institute of Aeronautics and Astronautics.
- [84] Andrea Saltelli, Marco Ratto, Thomas Andres, Francesca Campolongo, Jessica Cariboni, Domenico Gatelli, Michaela Saisana, and Stefano Tarantola. *Global Sensitivity Analysis: The Primer*. Wiley, 2008.
- [85] Pramudita Satria Palar, Eric Nguyen Van, Nathalie Bartoli, and Joseph Morlier. Design exploration of a distributed electric propulsion aircraft using explainable surrogate models. *Journal of Aircraft*, 61(5):1561–1574, 2024.
- [86] Paul Saves, Youssef Diouane, Nathalie Bartoli, Thierry Lefebvre, and Joseph Morlier. A mixed-categorical correlation kernel for Gaussian process. *Neurocomputing*, 550:126472, 2023.
- [87] Paul Saves, Youssef Diouane, Nathalie Bartoli, Thierry Lefebvre, and Joseph Morlier. High-dimensional mixed-categorical Gaussian processes with application to multidisciplinary design optimization for a green aircraft. *Structural and Multidisciplinary Optimization*, 67(5):81, 2024.
- [88] Paul Saves, Rémi Lafage, Nathalie Bartoli, Youssef Diouane, Jasper Bussemaker, Thierry Lefebvre, John Hwang, Joseph Morlier, and Joaquim Martins. SMT 2.0: a surrogate modeling toolbox with a focus on hierarchical and mixed variables Gaussian processes. *Advances in Engineering Software*, 188:103571, 2024.
- [89] Paul Saves, Nicolas Verstaev, and Benoit Gaudou. Modèles de substitution pour les modèles à base d'agents: Enjeux, méthodes et applications. In *33èmes Journées Francophones sur les Systèmes Multi-Agents*, volume 2025, pages 107–115, Dijon, France, 2025. Cépaduès.
- [90] Thomas Schelling. Models of segregation. *The American Economic Review*, 59(2):488–493, 1969.
- [91] Glenn Shafer and Vladimir Vovk. A tutorial on conformal prediction. *Journal of Machine Learning*

Research, 9(3), 2008.

- [92] Lloyd Shapley. Stochastic games. *Proceedings of the national academy of sciences*, 39(10):1095–1100, 1953.
- [93] Lloyd Shapley. A value for n-person games. In *Contributions to the Theory of Games, Volume II*, volume 28 of *Annals of Mathematics Studies*, pages 307–317. Princeton University Press, 1953.
- [94] James Shihua, Paul Saves, Rhea Liem, and Joseph Morlier. Bayesian optimization of a lightweight and accurate neural network for aerodynamic performance prediction. *arXiv preprint*, 2025.
- [95] Abhinav Singh, Dmitri Vainchtein, and Howard Weiss. Schelling’s segregation model: Parameters, scaling, and aggregation. *Demographic Research*, 21:341–366, 2009.
- [96] Jaroslaw Sobiesczanski-Sobieski. Sensitivity of complex, internally coupled systems. *AIAA journal*, 28(1):153–160, 1990.
- [97] Ilya Sobol’. Global sensitivity indices for nonlinear mathematical models and their Monte Carlo estimates. *Mathematics and computers in simulation*, 55(1-3):271–280, 2001.
- [98] Eunhye Song, Barry Nelson, and Jeremy Staum. Shapley effects for global sensitivity analysis: Theory and computation. *SIAM/ASA Journal on Uncertainty Quantification*, 4(1):1060–1083, 2016.
- [99] Patrick Taillandier, Benoit Gaudou, Arnaud Grignard, Quang Huynh, Nicolas Marilleau, Philippe Caillou, Damien Philippon, and Alexis Drogoul. Building, composing and experimenting complex spatial models with the GAMA platform. *GeoInformatica*, 23(2):299–322, 2019.
- [100] Patrick Taillandier, Arnaud Grignard, Nicolas Marilleau, Damien Philippon, Quang-Nghi Huynh, Benoit Gaudou, and Alexis Drogoul. Participatory modeling and simulation with the GAMA platform. *Journal of Artificial Societies and Social Simulation*, 22(2), 2019.
- [101] Franck Varenne. Simulation informatique et pluriformalisation des objets composites. *Philosophia scientiae*, 131(1):135–154, 2009.
- [102] Franck Varenne and Marc Silberstein. *Modéliser & simuler. Epistémologies et pratiques de la modélisation et de la simulation*, volume 1. Éditions matériologiques, 2013.
- [103] Haomiao Wang, Emmanuel Doumard, Chantal Soulé-Dupuy, Philippe Kemoun, Julien Aligon, and Paul Monserrat. Explanations as a new metric for feature selection: a systematic approach. *IEEE Journal of Biomedical and Health Informatics*, 27(8):4131–4142, 2023.
- [104] Alexander Wilhelm and Katharina A Zweig. Hacking a surrogate model approach to XAI. *arXiv preprint*, 2024.
- [105] Theodore Zamenopoulos and Katerina Alexiou. *Co-design as collaborative research*. Bristol University, 2018.